NASA TECHNICAL MEMORANDUM

NASA TM X-71675

SOLUTIONS FOR DISCHARGE CHAMBER SPUTTER-
ING AND ANODE DEPOSIT SPALLING IN
SMALL MERCURY ION THRUSTERS

by John L. Power and Donna J. Hiznay
Lewis Research Center
Cleveland, Ohio 44135

TECHNICAL PAPER to be presented at
Eleventh Electric Propulsion Conference sponsored
by American Institute of Aeronautics and Astronautics
New Orleans, Louisiana, March 19-21, 1975.

SOLUTIONS FOR DISCHARGE CHAMBER SPUTTERING AND ANODE

DEPOSIT SPALLING IN SMALL MERCURY ION THRUSTERS

by John L. Power and Donna J. Hiznay

Lewis Research Center
Cleveland, Ohio 44135

CONTENTS

SOLUTIONS FOR DISCHARGE CHAMBER SPUTTERING AND ANODE

DEPOSIT SPALLING IN SMALL MERCURY ION THRUSTERS

by John L. Power and Donna J. Hiznay

Lewis Research Center

I. INTRODUCTION

Proposed missions employing small electron bombardment mercury ion thrusters for attitude control and station-keeping of earth synchronous satellites could require operational lifetimes on the order of 20 000 hours for the thrusters (ref. 1). Such an operating duration may pose problems due to sputter erosion of thruster discharge chamber components. Severe erosion could impair the operation of a component or structurally weaken it to the point of mechanical failure. Furthermore, the deposits of sputtered material which build up in the discharge chamber may spall off in flakes. These can short out the anode, the cathode keeper, or the ion extraction grid system, or they may cause localized severe sputter erosion of the grids.

Since mercury ion thrusters are normally configured so that all discharge chamber components except the anode and the cathode keeper are at cathode common potential, the exposed surfaces of these components are subject to sputter erosion during thruster operation. The sputtering is produced by mercury ions accelerated across the plasma sheath by the sheath potential drop, given approximately by the discharge potential, ΔV_I. The material sputtered by these ions can only deposit on the anode without eventually being resputtered. The anode interior surface is therefore the site where the majority of the sputtered material ultimately deposits, and the spalling and flaking of sputtered deposits is essentially confined to this surface in small mercury ion thrusters.

Spalled flakes of sputter-deposited material in the discharge chamber have proven to be a serious problem during long-term thruster

operation. Such flakes caused the termination of an endurance test of a structurally integrated 5 cm diameter mercury ion thruster (SIT-5) after 9715 hours operation, as previously reported (ref. 2). They have also caused operational difficulty and some grid system damage in an endurance test of a 30 cm diameter mercury ion thruster after 5000 hours operation (ref. 3). However, this thruster has continued to operate and has accumulated a total of over 8000 hours running time.

A series of three 400-hour tests conducted with a SIT-5 thruster at constant ΔV_I's of 36.6, 39.6, and 42.6 V established (ref. 4) that the sputter erosion rates of nearly all the discharge chamber components rose with discharge voltage in the approximate ratio of 1:3:5 for these three ΔV_I's. (These tests are hereinafter referred to as the "ΔV_I erosion tests".) The erosion rate ratios over the investigated range of ΔV_I were found to correlate well with predicted production rate ratios for doubly charged mercury (Hg^{+2}) ions over a corresponding 21 to 28 eV range of the primary electron energy in the main discharge. This and other evidence strongly supported the conclusion that Hg^{+2} ions were the principal species responsible for the sputter erosion observed in the discharge chamber.

The results of the ΔV_I erosion tests suggested a method by which accelerated life testing could be accomplished and by which potential solutions to the problems of sputtering and sputter deposit spalling in the discharge chamber could be evaluated. The approach was to operate the 5 cm thruster continuously at a ΔV_I substantially increased from the normal value of 40 V. Such operation could be expected to greatly increase the sputter erosion rates of the internal discharge chamber components and cause correspondingly increased sputter-deposition on the anode, with attendant spalling of the sputtered coating.

The purpose of the investigations reported herein was to evaluate several proposed solutions to the problems of sputter erosion and sputtered material spalling in the discharge chamber of small mercury ion thrusters. The accelerated life test summarized in the following section evaluated three such proposed solutions: (1) the use of tantalum as

a single low sputter yield material for the exposed surfaces of the discharge chamber components subject to sputtering, (2) the use of a severely roughened anode surface to improve the adhesion of the sputter-deposited coating, and (3) the use of a wire cloth anode surface in order to limit the size of any coating flakes which might spall from it.

Because of the promising results obtained in the accelerated life test with anode surfaces roughened by grit-blasting, experiments were carried out to optimize the grit-blasting procedure. The experimental results and an optimal grit-blasting procedure are presented in section III of the report. In section IV, four sputter deposition tests, not conducted in the discharge chamber of a thruster, are described which evaluated both solid and wire cloth surfaces grit-blasted by the optimized procedure. These tests assessed the adhesion and spalling of sputtered coatings having compositions and thicknesses representative of actual discharge chamber conditions.

Finally, in section V two extended thruster tests are described in which graphite instead of tantalum has been employed as a low sputter yield material of which two discharge chamber components subject to sputtering were constructed. These components were the baffle and the exposed surface of the thruster backplate.

II. ACCELERATED LIFE TEST

An accelerated life test, motivated by the results of the earlier ΔV_I erosion tests (ref. 4), was conducted with a SIT-5 thruster modified so as to test tantalum as a low sputter yield surface material for the discharge chamber components subject to sputtering. In the modified SIT-5 thruster the exposed surfaces of all such components, apart from the molybdenum screen grid, were either constructed of, coated with, or covered by tantalum. Tantalum was chosen not only because of its indicated superior sputtering resistance under mercury thruster discharge conditions (ref. 3) but also because of its good forming characteristics.

Figure 1 shows a diagram of the thruster as tested, equipped as in the ΔV_I erosion tests with a dual axis electrostatic vectoring grid assembly (ref. 5). The specific modifications of the SIT-5 thruster which were incorporated for the accelerated life test included (1) use of tantalum foil covers over the exposed mild steel surfaces of the cathode pole piece; (2) replacement of the stainless steel baffle mounting screw with a specifically fabricated, thin head tantalum screw, installed with the head on the downstream side of the (tantalum) baffle; (3) use of a tantalum backplate cover; and (4) coating of the exposed nickel-plated surfaces of the anode pole piece insert with plasma-sprayed tantalum. Figure 2 shows the baffle and baffle mounting screw before the test. The entire cathode pole piece-baffle assembly with the tantalum foil covers installed is seen in figure 3. Figure 4 shows the rough, granular surface of the anode pole piece insert as plasma-sprayed with tantalum.

Several different test surfaces were employed on the interior of the anode during the accelerated life test to determine how well the sputter-deposited anode coating would adhere to different types of surfaces and what size coating flakes would spall from them. The evaluated surfaces were: (1) the smooth, virgin, polished surface of the type 304 stainless steel anode shell; (2) the same surface uniformly grit-blasted with a 50 μm particle size silicon carbide (SiC) abrasive powder, using a micro-sandblaster; (3) the smooth, virgin surface of a 0.05 mm thick tantalum foil insert; (4) the same surface as (3) (part of the same insert) uniformly grit-blasted by the same procedure used for the stainless steel surface above; and (5) a coarse, opaque, double woven stainless steel wire cloth insert (20 × 100 wires/cm) made of 0.20 to 0.25 mm diameter wire. All of these surfaces extended virtually the entire length of the anode. The entire anode assembly, with the tantalum foil and wire cloth inserts installed, is shown before the test in figure 5. Figures 6 to 8 show the grit-blasted and smooth stainless steel surfaces, the grit-blasted and smooth tantalum surfaces, and the stainless steel wire cloth surface, respectively, all before testing.

During the accelerated life test the SIT-5 thruster, modified as indicated above, was operated continuously for 200 hours at a ΔV_I of 64.6 V. The other controllable operating conditions were maintained essentially at standard values for the SIT-5 thruster. The more important operating conditions are given in table I. The discharge voltage of 64.6 V at which the test was run was determined from preliminary experiments. These established the result that 65 V was essentially the maximum value of ΔV_I at which the thruster could be operated stably over an extended period of time with the available power processing unit.

A detailed preliminary report describing the accelerated life test and its results is available (ref. 6).

A. Sputter Erosion

The discharge chamber components which suffered major erosion in the accelerated life test are given in table II with the weight each lost in the test. The components most severely eroded on a weight basis were the screen grid upstream surface (as estimated from the total grid assembly weight loss), the tantalum foil cover over the cathode pole piece tip, and the baffle. Figure 9 shows the severe sputter erosion evident after the test on the exposed downstream surface of the baffle, and figure 10 shows the corresponding edge view. Relative to its size, the baffle was the most heavily eroded component, losing 10 percent of its weight, 13 percent of its outer edge thickness, and 1.3 percent of its outside diameter during the test. The average absolute sputter erosion rate for the exposed downstream surface of the baffle was found to be ~ 0.54 mg cm^{-2} hr^{-1}.

The only individual discharge chamber components used without modification in both the accelerated life test and the previously conducted ΔV_I erosion tests (ref. 4) were the baffle and the screen grid. The sputter erosion rates measured or estimated for these two components may be compared between the ΔV_I erosion test at the

standard discharge potential of 39. 6 V and the accelerated test at 64. 6 V
to estimate the factor by which the erosion rates were increased in the
latter. Both such comparisons yield a factor of 75 increase in the ero-
sion rates at the higher voltage. Thus, assuming that sputter erosion is
linear with thruster operating time, the 200 hour accelerated life test was
approximately equivalent to 15 000 hours operation of the thruster at a
normal discharge voltage (39. 6 V), as far as sputtering of the discharge
chamber components is concerned.

None of the discharge chamber components was sputter eroded to
such an extent in the accelerated life test that its structural integrity or
further serviceability was at all threatened. (Neither tantalum foil
cathode pole piece cover is considered as a separate component in this
generalization. In three places the 0. 05 mm thickness of the pole piece
tip cover was eroded through during the test.) Indeed no component ap-
peared in danger of erosion to such extent for at least several times the
15 000 hour equivalent operating duration of the test. As described
earlier, the tantalum baffle was the component most seriously eroded
relative to its size. It also was indicated to be the first component to
fail due to sputtering damage on indefinitely extended thruster operation.

Despite some differences, the qualitative sputter erosion pattern
and characteristics observed in the accelerated life test agreed quite
well with those seen in the earlier ΔV_I erosion tests, which were con-
ducted at normal discharge voltages. These observations support the
validity of the accelerated life test concept.

B. Sputter-Deposited Anode Coatings

Examination of the anode assembly following the accelerated life
test revealed that the adhesion of the typically 3. 2 μm thick sputtered
anode coating generated during the test was much superior on the grit-
blasted anode test surfaces than on the smooth surfaces. Grit-blasting
of the surface clearly was the overriding factor determining the anode
coating adhesion. The sputtered coating adhered totally, without cracks,

flaws, or spalling, to both of the grit-blasted anode surfaces. The typical appearance of the coating on these surfaces is seen in the lower portion of figure 11, which shows the coated, grit-blasted tantalum surface following the test. Even severely stressing the coated, grit-blasted surfaces by shearing pieces from them caused no cracking or spalling of the coating to occur.

Both the smooth stainless steel and the smooth tantalum anode surfaces, on the other hand, showed extensive spalling of their sputtered coatings following the test. Figure 12 shows portions of both of these surfaces; the spalling and flaking of their coatings is evident. In fact, the sputtered coating on well over half the area of both of these surfaces had spalled off completely when examined after the test, and upon stressing the smooth surface of the tantalum insert by cutting out samples from it, much of the remaining coating separated in large flakes.

The dominant effect that grit-blasting the substrate surface has on the adhesion of the sputtered anode coating is well illustrated in figure 11. This photograph of the tantalum foil insert following the test shows that the boundary between the completely spalled region of the coating (upper portion of figure) and the completely adhered region (lower portion of figure) almost exactly coincides with the boundary between the smooth and the grit-blasted areas of the insert.

The sputtered coating on the coarse stainless steel wire cloth anode insert initially showed fairly good adhesion following the accelerated life test. However, on microscopic examination many cracks in the coating could be seen along the exposed wire crests. With time and extended exposure to air much of the sputtered coating on the exposed wire surfaces spalled off, leaving coating fragments on the individual wires of the insert which appeared as seen in figure 13 when viewed with a scanning electron microscope. On extensive examination of the spalled coating areas of the wire cloth insert, no evidence could be found of spalled flakes larger than a fraction of the surface mesh opening dimensions ($\sim 0.40 \times 0.50$ mm, measured between adjacent wire center lines). In fact, no cases could be found in which a

continuous coating extended from one wire of the cloth to an adjacent or crossing wire. The results of the accelerated life test indicate that the size of spalled anode coating flakes can be limited (provided the coating is thin compared to the limiting mesh dimensions) by employing a tightly woven wire cloth anode surface of appropriately small mesh size.

The thruster was horizontally oriented during the accelerated life test, and when it was disassembled afterwards a copious amount of loose coating flakes was found in it, particularly on the anode. A portion of these loose flakes is shown in figure 14. At least most of the flakes clearly were sections of the sputtered coating which had spalled off of the smooth anode surfaces. Though the flakes were of all sizes, many of the larger were over 1.0 mm long, much longer than necessary to short out the grid system or cause other serious problems. Generally smaller loose coating flakes were also found on the interior surface of the anode pole piece insert, as seen in figure 15. These and all the flakes collected were nonmagnetic.

The weight gained by the anode assembly during the accelerated life test, after removal of all loose flakes from it, was found to be 161.8 mg. The weight of all the loose material collected (with no allowance made for that unavoidably lost), plus the small to moderate weight gains shown by the anode pole piece insert, the cathode assembly shield (see fig. 1), and the thruster backplate (as distinct from the backplate cover), came to 38.6 mg. Hence the total weight increase from all sources in the discharge chamber during the accelerated life test was a minimum of 200.4 mg. This accounts for 93 percent or more of the total weight loss of 215.7 mg (including the estimated loss from the upstream screen grid surface) found for all the discharge chamber components which lost weight during the test.

The approximate agreement found between the total weight gained and that lost in the discharge chamber during the accelerated life test confirms a conclusion obtained in the earlier ΔV_I erosion tests (ref. 4). This is that relatively little sputtered material enters or

leaves the discharge chamber through the grid system during operation of the SIT-5 thruster, when equipped with an electrostatic vectoring grid assembly. This conclusion supports the previously noted similarity between the sputter erosion characteristics observed in the accelerated life test and those found in the ΔV_I tests at normal discharge voltages and further substantiates the accelerated life test concept. Hence it appears that operation of a small ion thruster at a substantially elevated ΔV_I will reproduce, at a much accelerated rate, the important features of the discharge chamber sputtering and sputter-deposition phenomena which occur during normal, uncycled thruster operation.

III. GRIT-BLASTING OPTIMIZATION

The accelerated life test demonstrated that the sputtered coating adhesion to the anode could be dramatically improved by grit-blasting the substrate surface. It also showed that a wire cloth anode surface could limit the size of any spalled coating flakes to the cloth mesh dimensions. For these reasons a systematic study was undertaken to optimize the grit-blasting procedure for both solid and wire cloth surfaces. It was expected that the grit-blasted wire cloth surfaces should combine the assets of good sputtered coating adhesion and of mesh dimension-limiting of the size of any spalled coating flakes.

The principal reason for the vastly improved adhesion of sputter-deposited coatings to grit-blasted as compared to smooth surfaces is certainly the much superior mechanical resistance to separation from the substrate by shearing and flexural forces. Since it was impractical to conduct sputter-deposition tests (such as described in the following section) to evaluate the effect of each grit-blasting variable, the arbitrary assumption was made that the roughest surface was the optimum surface for sputtered coating adhesion. On such a surface the mechanical adhesion of the coating should be maximized. Hence the goal of the grit-blasting optimization was to produce the roughest possible surfaces on both the solid and the wire cloth materials tested.

An operational definition of surface roughness is the ratio of true surface area to the projected normal area of a specimen. With this definition maximum surface roughness correlates with maximum surface feature depth, angularity, and density per unit area. These surface properties, as well as the surface feature size, were evaluated in the optimization experiments by examination and comparison of the grit-blasted surfaces using a scanning electron microscope (SEM). Magnifications up to 2000 times with the specimens usually tilted 60° with respect to normal incidence of the electron beam generally permitted good observation of the surface features. Figure 16 shows a SEM image (at ×700 magnification and 60° tilt) of a typical grit-blasted solid surface. In this case stainless steel was grit-blasted by approximately the same procedure used to prepare the grit-blasted anode shell surface employed in the accelerated life test. The size, depth, angularity, and density per unit area of the surface features seen in this figure are typical of those found for a heavily grit-blasted solid surface in the optimization study. Characteristic dimensions and depths of the surface features seen in figure 16 are both about 10 μm.

The apparatus used for preparing all the grit-blasted surfaces employed in the work reported in this paper was a commercial micro-sandblaster (ref. 7). This unit delivers a high velocity stream of microscopic abrasive particles in a jet of dry nitrogen gas emerging through a small diameter nozzle orifice. The abrasive powder is introduced into the carrier stream by magnetic vibration of the powder reservoir tank, with the powder entering the gas stream through an orifice plate. Control of the powder flow rate is achieved by control of the AC voltage governing the vibration amplitude.

The grit-blasting variables investigated in the optimization study and the range over which each was varied are shown in table III. Three to five values spanning the indicated range were tested for each of the continuous variables except for the angle of attack, the effect of which was evaluated only at the two angles shown in the table. In some

of the experiments two or three of the variables were varied together to investigate interaction effects.

The wire cloth surfaces tested in the grit-blasting optimization included (1) the coarse stainless steel cloth from which the wire cloth anode insert in the accelerated life test was fabricated and (2) a fine mesh, double woven stainless steel cloth (80 × 450 wires/cm), made of 0.045 to 0.050 mm diameter wire. Figure 17 shows the appearance of the fine mesh cloth under the SEM at ×700 magnification before grit-blasting or sputter deposition.

In general the test specimens were prepared by grit-blasting a 0.46 cm diameter spot on the substrate through a thin mask attached to it. After grit-blasting, each specimen was cleaned ultrasonically for 10 to 15 minutes in acetone and then for about the same period in high purity CCl_3CF_3 (Freon) before being examined with the scanning electron microscope. The ultrasonic cleaning was performed in an attempt to remove all residual grit-blasting particles and loose, eroded substrate material lodged in the surface after grit-blasting.

The results of the grit-blasting optimization experiments showed important effects due to some variables and minor effects due to others. As an example, comparison between grit-blasted surfaces prepared with silicon carbide (SiC) and aluminum oxide (Al_2O_3) abrasive powders of the same or nearly the same particle size indicated little choice between the two materials. The 50 μm SiC abrasive powder gave perhaps slightly rougher surfaces on the solid stainless steel and tantalum tested than did the 50 μm Al_2O_3, and the 27 μm Al_2O_3 gave somewhat rougher surfaces than the 25 μm SiC on the same substrates. However, a very large, more than linear difference in roughness was noted between the surfaces prepared with the 25 to 27 μm particle size powders and those prepared with the 50 μm powders of the same materials, with the latter surfaces much the rougher. This large effect due to particle size is seen in figures 18(a) and (b), which show solid stainless steel specimens grit-blasted with 50 and 25 μm particle size SiC, respectively, as viewed with the SEM under ×2000 magnification. In each case the grit-blasting time was 30 seconds, the

pressure was 55 N cm^{-2}, and the other grit-blasting conditions were at the optimized values listed in table III. The characteristic dimensions and depth of typical surface features seen in figure 18(a) are ~10 μm, while the comparable dimensions and depth of the surface features in figure 18(b) are about one quarter as large.

The 50 μm SiC abrasive powder used is shown in figure 19 at ×2000 magnification, the same magnification at which figure 18(a) was obtained. Comparison of these figures indicates the particle size of the 50 μm SiC abrasive powder is about five times the size of the typical grit-blasted surface features it produces in stainless steel. Evidently, the sharp corners and edges of the abrasive particles and the much greater hardness of the SiC, compared to the substrates grit-blasted, produce the angularity and roughness of the grit-blasted surfaces.

In a series of tests, various solid substrate materials were grit-blasted by a standard procedure to comparatively evaluate them for optimal surface roughness. The materials evaluated were type 304 stainless steel, tantalum, molybdenum, aluminum (type 5052), platinum, tungsten, titanium, and magnesium (alloy type AZ31B). The optimized grit-blasting prescription given in table III was used except that a pressure of 55 N cm^{-2} was employed.

The results of the solid substrate tests indicated that stainless steel, magnesium, aluminum, platinum, and tantalum yielded the best, that is, the roughest, surfaces from grit-blasting, with titanium somewhat inferior and tungsten and molybdenum substantially inferior. Possible small differences in roughness within these groupings were also indicated in the order listed. Figure 20(a) shows the stainless steel and figure 20(b) the molybdenum surfaces prepared in this series of tests, both viewed under ×2000 magnification at 60° specimen tilt in the SEM.

A property of the substrate metal which appears to correlate well with the roughness of its grit-blasted surface is the yield strength. This correlation is suggested by the surface roughness and appearance of the eight different metals comparatively grit-blasted. Of these, molybdenum and tungsten showed poorly roughened surfaces, compared

with the other metals. These two materials have far higher yield strengths (refs. 8 to 10) than the others. Their surfaces thus are presumably much more resistant to plastic deformation, hence much less penetrable, by the high velocity, sharp-edged, hard abrasive particles. Furthermore, surface features formed on these materials are likely to be more susceptible to removal by brittle fracture under further bombardment by the abrasive particles.

On solid stainless steel and tantalum substrates the variables of grit-blasting time and pressure were found to have no further effect on the roughness, appearance, and surface feature density of the grit-blasted surfaces, once a saturated or equilibrium condition of surface feature density had been attained. This unchanging equilibrium condition is demonstrated by figures 18(a) and 20(a). These show no evident change in the surface roughness or surface feature density of solid stainless steel specimens grit-blasted for 30 and 12 seconds, respectively. In both cases the other grit-blasting variables were at the optimized values listed in table III except that a pressure of 55 N cm^{-2} was employed for both specimens.

However, below the minimum saturation conditions of about 12 seconds grit-blasting time at 14 N cm^{-2} pressure and 5 seconds at 28 N cm^{-2}, the solid surfaces were found not to have reached an equilibrium surface structure. Figures 21(a) and (b) show this effect, depicting stainless steel surfaces grit-blasted at the optimized conditions of table III except that a grit-blasting time of 2 seconds was used in the case of the figure 21(a) specimen, while the figure 21(b) specimen was grit-blasted for the standard 12 second period. In both cases the SEM images were obtained at ×2000 magnification. Figure 21(a) clearly shows a surface which is unsaturated with regard to grit-blasting effects.

Within the ranges indicated in table III, the grit-blasting variables of nozzle to specimen distance, nozzle orifice size, and feed rate were not found to have any significant effect on the surface roughness, appearance, or density of grit-blasted features on solid stainless steel

specimens. These specimens were grit-blasted for 12 seconds at pressures of 14, 28, and 55 N cm^{-2}. Evidently for each of the three variables mentioned the least intense grit-blasting condition tested was more than adequate to achieve surface feature saturation on the test specimens.

In evaluating the effect of the grit-blasting angle of attack, a solid stainless steel specimen was grit-blasted at a 45° angle with the other variables, apart from the pressure, at the optimized levels shown in table III. A pressure of 55 N cm^{-2} was employed for the test. The surface thus prepared, shown in figure 22, may be compared with the corresponding surface grit-blasted at 90°, seen in figure 20(a) at the same magnification. The 45° grit-blasted surface showed a lower density of surface features and shallower contours than the surface prepared at normal incidence. It also displayed some long surface grooves not seen on the latter surface. From these comparisons a 90° angle of attack appeared to produce the roughest, hence optimum, grit-blasted surface.

All the described effects of the grit-blasting variables that were noted in preparing solid stainless steel surfaces were also evident in grit-blasting the coarse and the fine stainless steel wire cloths. However, with the wire cloths an additional important characteristic was observed. After the point of surface feature saturation was reached, further extensive grit-blasting led to an undesirable, excessively eroded condition, particularly in the case of the fine mesh wire cloth.

This effect may be seen in figures 23(a), (b), and (c). These are SEM images at ×700 magnification of the fine mesh stainless steel wire cloth grit-blasted at the optimized conditions of table III except that pressures of 14, 28, and 41 N cm^{-2}, respectively, were employed for the three samples. Surface feature saturation on the exposed portions of the wires was evidently just achieved in the low pressure case (fig. 23(a)). The specimen prepared at the intermediate 28 N cm^{-2} pressure (fig. 23(b)) shows surface erosion mildly in excess of a saturated surface feature condition. The specimen shown in figure 23(c),

which was grit-blasted at the moderately high pressure of 41 N cm^{-2}, displays a considerable degree of excessive erosion in several evident features. These include (1) substantial flattening of the exposed wire surfaces due to preferential erosion of the outermost wire material, (2) bridging between crossing wires, with consequent loss of definition of the individual wires, and (3) apparent trapping in the mesh openings of remnant particles of both the grit-blasting abrasive powder and eroded material from the wire cloth. On even more extensive grit-blasting than shown in figure 23(c) the fine mesh wire cloth appeared as a single, flat, grit-blasted surface with regularly spaced holes partially filled in with grit-blasting debris.

Despite the extensive ultrasonic cleaning to which the test specimens were subjected after being grit-blasted, SiC from the abrasive powder was still found to remain lodged in the grit-blasted surfaces. This was true for both the solid and the wire cloth samples. The presence of the abrasive material was detected by SEM X-ray analysis, though no actual particles of the abrasive could be found. It thus appears to be difficult to completely remove all fragments of the abrasive powder from a grit-blasted surface, especially a fine mesh wire cloth surface.

Some small degree of grit-blasting of the wire cloth surface beyond surface feature saturation, as in figure 23(b), appears to be advisable to insure that the partially concealed wire surfaces inside the mesh openings are roughened at least to a moderate extent. For the fine mesh wire cloth tested, the wire edge to wire edge spacing of ~45 μm across the surface mesh openings suggests that the ~50 μm diameter abrasive particles can barely, if at all, enter the mesh openings to impinge on the partially concealed wire surfaces. Hence the observed difficulty in roughening these surfaces with the 50 μm abrasive powder is understandable. The other effects associated with excessive grit-blasting of the fine mesh wire cloth surfaces all appear to be undesirable for improving the adhesion of sputtered coatings. These considerations therefore indicate that the optimum grit-blasting

conditions for preparing fine mesh wire cloth surfaces should produce a minimally overeroded surface.

Several other grit-blasting variables listed in table III had effects comparable to that of the pressure in causing excessive erosion of the fine mesh stainless steel wire cloth. Increasing the grit-blasting time, decreasing the nozzle to specimen distance, decreasing the nozzle orifice size, and increasing the feed rate all led to the same overeroded condition depicted in figure 23(c).

Hence the optimal grit-blasting conditions recommended and specified in table III were chosen to achieve surface feature saturation on the exposed substrate surfaces, produce moderate roughening of the partially concealed wire surfaces of the wire cloths evaluated, and yet avoid more than moderate overerosion of the highly exposed wire surfaces of these wire cloths. The prescription should be applicable to all solid metal surfaces behaving like stainless steel upon grit-blasting and to all stainless steel wire cloths of mesh size greater than or equal to that of the fine mesh cloth tested in this work.

The grit-blasted tantalum and stainless steel anode test surfaces employed in the accelerated life test previously described were prepared by a grit-blasting procedure differing in three respects from the optimized prescription detailed in table III: the pressure used was 55 N cm^{-2}, the nozzle to specimen distance was about 0.6 cm, and the effective grit-blasting time is estimated to have been about 2 seconds. As viewed with the SEM the grit-blasted surfaces produced under these conditions were saturated in surface feature density and appeared very similar to the stainless steel surface depicted in figure 16. Hence the grit-blasted tantalum and stainless steel anode surfaces evaluated in the accelerated life test closely resembled the optimally grit-blasted solid surfaces prepared in the experiments reported in this section.

IV. SPUTTER DEPOSITION TESTS ON OPTIMIZED SURFACES

The optimized grit-blasting procedure developed in the experi-
ments described in the preceding section was tested for its effectiveness
in promoting sputtered coating adhesion in four sputter deposition tests.
These were not conducted in the discharge chamber of an ion thruster
but utilized instead the ion beam of an 8 cm diameter mercury thruster
(ref. 11) to produce the desired flux of sputtered material from a tar-
get of appropriate composition placed in the beam. The experimental
arrangement employed is shown in figure 24. As seen in the figure, the
grit-blasted test samples were mounted so as to receive the maximum
flux of sputtered material from the sputter target while at the same
time being shielded from direct impingement of the ion beam itself.
For all the tests the thruster was operated at its normal conditions of
1200 V net ion beam accelerating potential and 72 mA beam current.
A typical pressure of ~10^{-6} torr was maintained during the tests in
the vacuum facility employed.

For the first two sputter deposition tests pure tantalum sputter
targets were used to simulate the sputtered material generated in a
modified thruster having tantalum surfaces on all the discharge cham-
ber components sputtered. Except for its molybdenum screen grid
the thruster evaluated in the accelerated life test fitted this description.
In the third sputter deposition test a pure graphite target was used to
observe the characteristics of sputtered coatings of this material,
since it was under active evaluation for use in fabricating heavily sput-
tered discharge chamber parts such as the baffle. In the final sputter
deposition test reported a composite target including tantalum, graphite,
and other materials was employed to simulate the actual sputtered ma-
terial composition expected in the discharge chamber of a modified
8 cm diameter thruster currently undergoing a cycling endurance test.

As indicated in table IV, the substrate materials evaluated as
deposition surfaces in the sputter deposition tests included solid stain-
less steel and tantalum and the coarse and fine mesh stainless steel
wire cloths tested in the grit-blasting optimization study. These mate-

rials were prepared by grit-blasting according to the optimized prescription of table III except that grit-blasting pressures of 14, 28, and 55 N cm^{-2} were variously employed for the samples in the different tests, as shown in table IV. Sections of both the grit-blasted and the virgin, nongrit-blasted surface areas of each test sample were exposed to deposition in the sputtering experiments. Other sections of both these surfaces were protected with polyimide tape from any deposition during the tests to provide control surfaces. Before each test was run, all the specimens to be tested were ultrasonically cleaned by the procedure used in the grit-blasting optimization study.

Following a sputter deposition test, the four sections of each test specimen - two grit-blasted, two nongrit-blasted, two sputter-coated, and two not coated - were examined with the SEM. Frequently, examination of the boundaries between the four different regions on each specimen provided especially interesting and useful information. Such investigation, together with SEM observation of the edges of spalled coating flakes still attached to the specimens, allowed the thickness or thickness range of the sputtered coating deposited in each test to be determined. Following SEM examination, the samples from two of the tests were also mechanically stressed and thermally cycled to determine what effects this would have on their sputtered coatings.

For each of the four sputter deposition tests, table IV lists the grit-blasted samples exposed, the pressure at which the samples were grit-blasted, the composition of the sputtered target, the hours of 8 cm thruster operation as the ion source, the average thickness or the thickness range of the sputtered coating generated on the test specimens, and the approximate operating time of a small (5 or 8 cm diam) mercury ion thruster required to generate a sputter-deposited anode coating of the same thickness. This estimated small thruster operating time presumes appropriate modifications to the discharge chamber component surfaces so as to produce the same sputtered material composition as in the test. These equivalent operating times were estimated by comparison of the deposited coating thicknesses generated in the first two

sputter deposition tests with the coating thickness found in the accelerated life test. The results of the four sputter deposition tests are individually described and discussed below.

A. Thick Tantalum Sputter Deposition Test

The first sputter deposition test employed a pure tantalum target. Deposition took place on test samples of all four materials under evaluation. Specimens grit-blasted at each of the three pressures listed in table IV were tested for each material. The test produced sputtered tantalum coatings ranging in thickness from 18 to 29 μm. Based on the anode coating thickness measured in the accelerated life test, an anode coating in this thickness range would be generated in $\sim 1\times 10^5$ hours of small thruster operation at normal operating conditions, if the thruster were modified so that all its discharge chamber components subject to sputter erosion had tantalum surfaces. Such an equivalent operating time and such an anode coating thickness (of tantalum) presumably are substantially beyond the requirements of any near-term mission employing small mercury ion thrusters. The sputtered coatings generated in this test were considerably thicker than those produced in any of the other sputter deposition experiments. Their thicknesses were two to three times as great as the typical 10 μm surface feature dimension of the grit-blasted deposition surfaces being tested. Despite this fact, the coatings generally adhered well to the grit-blasted surfaces.

Following the deposition test, the coated test samples were cut with shears to prepare specimens for SEM examination. This operation was observed to subject the coatings to severe mechanical stresses, especially near the sheared edges. Hence an unintended mechanical test of the coating adhesion was performed in preparing the SEM specimens. In the subsequent sputter deposition tests this was avoided.

The tantalum coating on the solid stainless steel test samples was observed to be extensively spalled from the nongrit-blasted sample areas

when the samples were retrieved from the sputter deposition. The coating on the grit-blasted areas was completely adherent. On shearing the samples to prepare specimens for SEM examination the sputter-deposited coating spalled completely from the nongrit-blasted sample areas on all three solid stainless steel specimens, and portions of the coating on the grit-blasted areas near the sheared edges also spalled off. The specimens, as thus prepared, appeared as seen in figure 25(a).

The sputter-deposited coating on the nongrit-blasted areas of the solid tantalum samples, as obtained from the test, showed extensive cracking and incipient separation from the substrate, as well as some areas actually spalled off. The coating on all the grit-blasted areas was completely adherent and intact. On shearing the samples to prepare the SEM specimens, more of the coating on the nongrit-blasted areas spalled off but most of it remained attached, though apparently loose. In addition, almost the entire coating on the substrate area grit-blasted at a pressure of 28 N cm^{-2} spalled off completely, though the coating on the other grit-blasted sample areas was not significantly affected. The appearance of all the tantalum test specimens as prepared for SEM examination is seen in figure 26(a).

The coated grit-blasted regions of both the fine and the coarse wire cloth test samples showed no spalling of the sputtered coating when the samples were removed for observation. The nongrit-blasted regions of the samples showed minor spalling of the coating in microscopic flakes. In shearing the test samples to prepare specimens for SEM examination the coatings on the grit-blasted areas were essentially unaffected. Those on the nongrit-blasted areas, however, mostly spalled off the coarse wire cloth specimens and spalled to a moderate extent from the fine mesh specimens. In neither case were any of the spalled flakes macroscopic, that is, several mesh units, in size.

A general characteristic noted on all the test samples was that spalling of the sputtered coatings on the nongrit-blasted regions extended only to or slightly beyond the boundaries of the grit-blasted

areas. This lack of spalling propagation across the grit-blasting bound-
ary demonstrates that even for sputtered coatings as much as 30 μm
thick the coating adhesion is so improved by grit-blasting the substrate
surface as to overcome the lateral cohesive forces in the coatings them-
selves.

SEM examination of the coated test samples from the sputter depo-
sition test revealed another general characteristic. The surface rough-
ness and appearance of all the grit-blasted substrate surfaces propagated
with little change through the sputtered coatings and was well replicated
in the exposed coating surfaces. Figure 27(a) demonstrates this behavior,
showing at ×700 magnification a broken edge of the sputtered coating on
the solid stainless steel sample grit-blasted at 14 N cm^{-2}. Figure 27(b)
similarly shows, at ×2000 magnification, a broken coating edge on the
solid stainless steel sample grit-blasted at 28 N cm^{-2}. Though some
filling in and rounding off of the substrate surface features is evident
in the coating surface seen in figure 27(b), the preservation and propa-
gation of the grit-blasted surface features in the surface of the coating
is impressive.

Figure 28(a) shows a SEM image, at ×700 magnification, of the
boundary between the sputter-coated and the noncoated fine stainless
steel wire cloth surface grit-blasted at 14 N cm^{-2}. Here the filling
in and rounding of the original substrate surface features is more no-
ticeable, yet the original surface roughness is still fairly well pre-
served. In figure 28(b) at the same magnification the sharp change in
roughness and appearance of the coating surface at the grit-blasting
boundary is evident on the fine mesh wire cloth sample grit-blasted at
14 N cm^{-2}.

Figure 29 shows a SEM view at ×2000 magnification of the under
surface of a coating flake which spalled from the solid tantalum sample
grit-blasted at 14 N cm^{-2}. The surface is nearly indistinguishable from
the original grit-blasted surface on which the coating was deposited.
The figure thus reflects a very uniform, fine-grained deposition of sput-
tered material during the test, without subsequent crystallization or

modification of this material. Such deposition is also implied by the
preservation of the original grit-blasted surface features through the
thick coating deposited in the test.

The fact that the grit-blasted substrate surface texture and features,
perhaps 10 μm in typical size and depth, propagate through a sputtered
coating two to three times as thick has important implications regarding
the adhesion of sputtered coatings to such grit-blasted surfaces in mer-
cury ion thrusters. It implies that the adhesion of newly sputtered ma-
terial deposited on an existing sputtered coating should not change much
as the coating thickness increases, even if the composition of the sput-
tered material changes. Thus, layers of sputtered material deposited
on a sputtered coating already of substantial thickness (on a grit-blasted
substrate) should not show an enhanced tendency to spall from the un-
derlying coating. Also, even a thick coating on a roughened surface
should possess substantial resistance to spalling under applied thermal
or mechanical stress. This is because the coating remains mechanically
bonded to itself and to the grit-blasted substrate and because extended
slip or cleavage planes are absent. The very fact that the surface of a
sputtered coating of substantial thickness replicates a microscopically
rough substrate surface implies that the sputtered material deposits
and remains predominantly in an amorphous condition.

Figures 30(a) and (b) shows profile and surface views, respectively,
of the cracked and partially spalled tantalum coating on nongrit-blasted
areas of the fine stainless steel wire cloth samples. Both SEM images
were obtained at ×2000 magnification on sections of the coated specimens
grossly stressed during shearing of the samples to prepare the SEM
specimens. The profile of the sputtered coating seen in figure 30(a) is
of interest, showing the expected maximum thickness of the coating at
near normal incidence to the top surface of the wire cloth. This maxi-
mum thickness is seen to be ~60 percent of the wire diameter.

Figure 30(b) shows that, despite its relative thickness, the sput-
tered coating is barely continuous between adjacent, tangent cloth wires.
The crack evident in the coating does not extend from the coating on one

wire to that on an adjacent one. Another feature visible in the figure is the irregular shoulder of sputtered material visible on the adjacent sides of the wires deep in the mesh openings. Such shoulders are also visible in figure 28(b).

Figure 31 shows a SEM image, at ×200 magnification, of the spalled but still partially attached sputtered coating found on a nongrit-blasted region of one of the coarse stainless steel wire cloth specimens. The raised coating sections on the top of each wire are seen to have broken away from the coating on the sides of the wires at about the same angle from the normal to the cloth surface. This suggests that the size of spalled coating flakes under these circumstances should be fairly uniform and limited to a fraction of a mesh dimension.

After the 12 specimens from the sputtering test had been examined with the SEM, as discussed above, they were mechanically stressed by a standard procedure. This consisted of twice bending them lengthwise as tightly as possible around the circumference of a 0.64 cm diameter rod, with the sputtered coatings on the outside (under tension). After each bending the specimens were gently straightened to their original flat condition. Such mechanical stressing of the specimens constituted a fairly severe test of the coating adhesion to the substrates, as well as of the coating cohesion. Stressing the coated specimens had the following effects on them.

The solid stainless steel specimens all lost additional coating sections of moderate extent during the bending test. These spalled from the boundaries of the coated regions on the grit-blasted sample areas, which were the only areas of the stainless steel samples that obtained the sputter-deposited coating on preparation of the original SEM specimens. This spalling thus widened the bands along the specimen edges from which the coating was completely removed but still left intact the coatings on the major central sections of the grit-blasted sample areas. Apparently contributing to the additional spalling were residual effects from the severe stressing which the coating edge sections underwent during shearing of the samples to prepare the SEM specimens.

The solid tantalum specimens showed few effects from the mechanical stressing except that the entire sputtered coating on the specimen area grit-blasted at 14 N cm^{-2} spalled off. The cracked coating sections still attached to the nongrit-blasted areas of the tantalum specimens were not removed by the test.

The mechanical stressing caused no apparent spalling of the sputtered coating from the fine stainless steel wire cloth specimens but did apparently cause extended cracks in the coating. Some of these are seen in figure 32, which shows a SEM image at ×500 magnification of the coating on the fine mesh wire cloth sample area grit-blasted at 28 N cm^{-2}. On this specimen the coating is seen to be sufficiently connected between adjacent cloth wires that continuous cracks in it have developed roughly following the hidden transverse wires. These cracks probably indicate the locations of maximum shear strain between adjacent wires during the mechanical stressing.

The mechanical stressing test caused much of the sputtered coating on the grit-blasted areas and nearly all of the coating on the nongrit-blasted regions of the coarse stainless steel wire cloth specimens to spall off in small flakes. None of the spalled flakes were observed to be more than a fraction of a mesh unit in largest dimension. The coating on the specimen area grit-blasted at 55 N cm^{-2}, however, remained adherent and intact to the boundary of the grit-blasted region.

After being mechanically stressed as described above, the specimens from the sputtering test were thermally cycled to determine the effects of thermally induced stress on the sputtered coatings. The thermal cycling test consisted of heating the specimens in air to 250° C for 1 hour, allowing them to cool and remain at room temperature for 20 minutes, then repeating this treatment two more times. The high temperature chosen is believed to be about the maximum that the anode reaches during operation of the 5 or the 8 cm ion thrusters. With one exception the thermal cycling test had no significant effect on the sputtered coatings on any of the test specimens. The exception was that it resulted in completing the spalling of the coating from the nongrit-blasted regions of the coarse stainless steel wire cloth specimens.

Figures 25(b) and 26(b) show photographs of the solid stainless steel and solid tantalum test specimens after completion of the thermal cycling tests. By comparison of these views with figures 25(a) and 26(a) of the same specimens before the mechanical stressing and thermal cycling tests it is seen that these tests basically had little effect on the test specimens shown. One exception was that they did result in the detachment of the coating on the tantalum specimen area grit-blasted at 14 N cm^{-2}. The adhesion and integrity of the sputtered coatings on all the grit-blasted solid stainless steel specimen areas and on the tantalum specimen area grit-blasted at 55 N cm^{-2} thus remained good throughout all the experiments performed on the coated specimens. After all these tests the sputtered coatings adhering to the grit-blasted regions mentioned still were continuous and free of macroscopic cracks or sections separated from the substrates. Apart from the edge regions of the coatings, which were grossly stressed during initial shearing of the samples, these coatings also retained their continuity to essentially the boundaries of the grit-blasted regions on which they were deposited.

The coated specimens from this first sputter deposition test, together with the results of the stress experiments subsequently performed on them, clearly demonstrated the superior adhesion of the thick sputtered tantalum coatings generated in the test to coarsely grit-blasted, fine mesh stainless steel wire cloth. Though cracked in places, the coating remained securely attached throughout the performed operations to essentially the entire grit-blasted area of each of the fine mesh wire cloth specimens. In fact it remained similarly attached to most of the nongrit-blasted regions of these specimens as well. The adhesion of the sputtered coating to both of the corresponding regions on the coarse wire cloth specimens was clearly and significantly poorer than to the respective areas on the fine wire cloth specimens.

So little of the sputtered coating spalled from the grit-blasted fine mesh wire cloth surfaces through all the above-described operations that it could not be determined if coating flakes spalling from this surface would be limited in size to the mesh dimensions. The continuous

coating and coating cracks across distances of several mesh dimensions seen in figure 32 suggest that the tantalum coating generated in this sputter deposition test, being ~60 percent as thick as the wire diameter, was perhaps too thick for the size of all spalled coating flakes to be effectively limited by the mesh dimensions. However, for the coating on the nongrit-blasted fine mesh wire cloth regions, the size of spalled coating flakes did appear to be so limited. This also was the case for both the grit-blasted and the nongrit-blasted coated areas of the coarse wire cloth specimens.

The adhesion of the thick sputtered tantalum coating to the grit-blasted solid stainless steel surfaces evaluated in the test was indicated to be quite good. It was clearly better than the coating adhesion to the corresponding grit-blasted surfaces of the solid tantalum specimens under the conditions of the mechanical stress test. The tantalum coatings, though cracked and partially spalled, displayed curiously strong adherence to the nongrit-blasted solid tantalum surfaces, however. These specimens were the exception to the general observation that the sputtered coating adhesion to the grit-blasted specimen surfaces was definitely better, generally much better, than to the nongrit-blasted areas of the same specimens.

On both the solid tantalum and the coarse stainless steel wire cloth test samples evaluated in the sputter deposition test (and in the subsequent experiments performed) the areas grit-blasted at $55\,\mathrm{N\,cm}^{-2}$ retained their sputtered coating better than did the specimen areas grit-blasted at 14 and at $28\,\mathrm{N\,cm}^{-2}$. It is not clear that this is a reproducible result, however, and from the considerations raised in the preceding section suggesting that excessive erosion during grit-blasting of wire cloth anode surfaces is undesirable, it is still believed preferable to grit-blast at $28\,\mathrm{N\,cm}^{-2}$ than at $55\,\mathrm{N\,cm}^{-2}$. Apart from the two instances referred to, no significant effect of the grit-blasting pressure was observed in the results of the sputter deposition test.

B. Thin Tantalum Sputter Deposition Test, Mission Equivalent

The second sputtering test listed in table IV was also carried out with a pure tantalum target. Deposition surfaces of solid stainless steel, solid tantalum, and the fine mesh stainless steel wire cloth were evaluated in the test. Specimen areas grit-blasted at 14 and at 28 N cm^{-2} on each sample were exposed to deposition of the sputtered tantalum.

This test was designed to produce sputtered tantalum coatings of a thickness more commensurate than that generated in the first sputter deposition test with actual deposition thicknesses expected in a small thruster discharge chamber during a normal mission lifetime. Again the presumption was made that all the sputtered surfaces in such a thruster were fabricated of tantalum. A calculation of the appropriate length of time to conduct the sputter deposition under the same conditions as those in the first test was made based on the sputtered coating thicknesses found in the earlier test and in the accelerated life test.

The second sputter deposition test was also intended to evaluate the effects of a specific space mission requirement on the adhesion of the sputtered anode coating in the small thruster modified as mentioned. These are the effects due to ground testing the thruster for a few hours and then exposing the freshly deposited anode surface coating to air at atmospheric pressure before commencing a space flight. Surface oxidation of the coating or other effects due to the exposure to air could significantly alter the adhesion of the sputtered material subsequently deposited on the anode surface.

For unknown reasons the actual average coating thickness generated in the second sputter deposition test, 2.3 μm, was somewhat less than expected from the coating thicknesses generated in the first test. Still, on the basis of the accelerated life test results, it corresponded to the sputter deposition expected in ~1×10^4 hours operation of a (modified) 5 or 8 cm diameter thruster. This is a representative mission lifetime requirement. The ground testing simulation performed

in the sputtering test consisted of operating the 8 cm thruster used as the sputtering ion source for 30 seconds at the beginning of the test, then exposing the test specimens to air at atmospheric pressure for a few hours before completing the test. The 30 seconds of sputter deposition corresponds to that expected in ~20 hours of ground test operation of the (modified) small thruster.

Another change was made for the second sputter deposition test from the procedure employed in the first test. This was to prepare and mount the test specimens for the sputter deposition in the experiment so that they could be directly examined afterwards in the SEM. This procedural change, also employed in the final two sputtering tests, avoided shearing the coated samples to prepare specimens for SEM examination. Such shearing after the first sputtering test had been observed to subject the sputtered coatings to severe stresses and cause substantial spalling of them.

The results of the second sputter deposition test and the appearance of the coated samples were quite consistent with those of the first test (which likewise employed a tantalum target), taking into account the much reduced thickness of the coatings deposited in the second test. The sputtered coating generated in the second test was found to adhere without any spalling, cracking, or flaws to all the grit-blasted specimen surfaces tested. The coating was observed to be adherent over the entire grit-blasted area of each specimen. In addition, it was similarly well adhered to the nongrit-blasted regions of the fine mesh wire cloth specimens tested.

On all the samples of both solid materials evaluated in the test, cracks in and spalling of the coating deposited on the nongrit-blasted areas were found to have propagated exactly to the boundaries of the grit-blasted regions. Figure 33 depicts a typical example of this, showing a SEM view, at ×500 magnification, of the coated boundary region on the tantalum specimen grit-blasted at 28 N cm^{-2}. The tendency may also be noted in figure 33 for the coating on the nongrit-blasted surface of the tantalum specimen to curl downward on separating from the substrate. This was found to be characteristic of the tantalum specimens.

The initial surface roughness and appearance of the grit-blasted sample areas sputter-coated in the second sputter deposition test were found to propagate through the deposited coatings even more precisely than in the case of the thicker coatings in the first test. This accurate surface replication is well demonstrated by the nearly identical appearance of the SEM images in figures 34(a) and (b). These show views at ×2000 magnification of non-coated and coated areas, respectively, of the solid stainless steel test specimen surface grit-blasted at 28 N cm^{-2}. Figure 35 shows the appearance of the coated fine mesh wire cloth grit-blasted at 14 N cm^{-2}, also as viewed with the SEM at ×2000. The precise surface feature replication and propagation through the deposited coating evident in figures 34(a), 34(b), and 35 is not surprising for this sputter deposition test considering the thinness of the deposited tantalum layer. Its thickness was only ~25 percent of the typical surface feature dimension and depth for the grit-blasted surfaces tested.

Exposure of the test specimens to air after 30 seconds of sputter deposition in the test evidently had no adverse effect on the general bonding strength of the sputter-generated coatings to the grit-blasted test surfaces. Nor was any surface layering observed with the SEM in edge views of the coatings from the test. Such layering might have occurred from the atmospheric exposure. However, it is possible that the exposure of the nascent coatings to air did play a significant role in the cracking and spalling which the final coatings displayed on the nongrit-blasted areas of the solid test specimens. The air exposure may also have been important in the curling observed of the coating which cracked and separated from the smooth portions of the solid tantalum specimens, as seen in figure 33.

No significant effect due to grit-blasting pressure could be identified in the results of this sputter deposition test between the specimens grit-blasted at 14 and at 28 N cm^{-2}.

C. Graphite Sputter Deposition Test, Mission Equivalent

The third sputter deposition test listed in table IV employed a pure graphite target. The sputtered graphite was deposited on stainless steel specimens grit-blasted at 14 and at 28 N cm^{-2} pressure. The specimens consisted of solid sheet and both the fine and the coarse wire cloths. All the specimens were pre-cut and mounted for the sputter deposition so they could subsequently be examined directly with the SEM. The target material sputtered in the experiment was aniso-tropic pyrolytic graphite (ref. 12) of high purity, oriented with the graphite atomic layers perpendicular to the impinging ion beam. The experimental arrangement and conditions for the sputter deposition were the same as for the first two sputter deposition tests and the ion source was operated for the same length of time as in the second test. The 1.0 μm thickness of graphite deposited on the specimens in the test thus very roughly approximates the anode deposit thickness ex-pected in 10^4 hours operation of a small thruster modified to have anisotropic pyrolytic graphite surfaces on all its sputtered discharge chamber components.

Because of its indicated superior sputter resistance to mercury ions (ref. 13), graphite has been employed and tested in small mer-cury ion thrusters as the surface material of discharge chamber com-ponents subject to heavy sputter erosion. Two such tests are subse-quently described in this paper. The objective of the graphite sputter deposition test was to investigate the properties and characteristics of sputtered graphite coatings on candidate anode surfaces.

The low sputter yield of graphite to mercury ion sputtering is re-flected in the much reduced thickness of graphite deposited in this deposition test as compared with the thickness of tantalum generated in the second sputter deposition test. Both tests were run under es-sentially identical conditions and for the same length of time.

The thin, matte black graphite coating generated in the graphite sputter deposition test was observed to show as poor or poorer ad-hesion to the exposed nongrit-blasted specimen surfaces as did the

thicker tantalum coatings generated in both of the tantalum deposition tests. However, the graphite coating demonstrated total adhesion to the grit-blasted specimen areas with no cracking or spalling. On all the specimens, particularly the solid specimens, spalling and cracking of the deposited coatings on the nongrit-blasted areas was observed to extend almost exactly to the boundaries of the grit-blasted regions, where both processes stopped. A good example of this and view of the graphite film generated in the test is seen in figure 36, which shows a SEM image at ×200 magnification of the coated boundary region on the solid stainless steel specimen grit-blasted at 14 N cm^{-2} pressure.

The graphite coating on all the solid stainless steel specimen areas not grit-blasted was found to be generally spalled, with the separated coating sections and flakes tending to curl both upwards and downwards at their edges. This tendency is evident in figure 36. The coating on the nongrit-blasted wire cloth specimen areas showed much less tendency to break off completely from the substrate wires but instead developed many cracks which propagated along the exposed wire crests for distances of less than a mesh unit. Actual spalling of the cracked coating from these specimen areas as flakes was observed only on the coarse mesh wire cloth specimens. None was seen from the fine mesh wire cloth specimens.

The coated, grit-blasted surfaces of the test specimens in the graphite sputter deposition test showed especially sharp replication and propagation of the original grit-blasted substrate surface features and contours, as a result of the thinness of the deposited coating. In the case of the fine mesh wire cloth specimens, however, coated grit-blasted areas were found having a surface appearance even rougher on a microscopic scale than the original grit-blasted surfaces. Figures 37(a) and (b) show SEM views at ×700 and ×2000 magnification, respectively, of such a coated area on the fine mesh wire cloth specimen grit-blasted at 14 N cm^{-2}. The apparent vertical projections of deposited material and the extreme asperity visible in figure 37(b) are not truly

representative of the grit-blasted surface (cf. fig. 35, for example), and it is not clear whether they are a genuine characteristic of sputtered graphite deposition on the grit-blasted fine mesh wire cloth. Such features, irregularly observed in the sputter deposition tests on other specimens, both solid and wire cloth, may be anomalous. They may in fact be due to the deposition of products from the underside adhesive of the polyimide tape used to shield part of each specimen from sputter deposition. In some places the edge of this tape was raised, partially exposing the adhesive. Whatever their origin, though, the features mentioned did not apparently affect adversely the cohesion of the coating or its adhesion to the grit-blasted substrate.

Mechanical stressing of the graphite-coated test specimens by the same procedure used on the specimens from the first tantalum sputter deposition test did not significantly affect the coatings on any of the grit-blasted areas. No spalling or cracking of the coatings on these regions was observed as a result of the procedure. The mechanical stressing did however cause all the remaining coating sections on the nongrit-blasted areas of the solid specimens to spall off. It also resulted in the general separation and removal of the coating from the nongrit-blasted areas of both the coarse and the fine mesh wire cloth specimens, except that on the former the coating on the partially shielded, steeply inclined wire surfaces deep within the mesh openings remained intact through the operations performed. On all the test specimens the spalled regions observed after the mechanical stressing were accurately defined by the boundaries of the grit-blasted areas. None of the coating flakes which spalled from the nongrit-blasted areas of the wire cloth specimens due to the bending test were indicated to be more than a fraction of a mesh unit in length.

Following the mechanical stressing of the graphite-coated test specimens they were thermally cycled by the same procedure employed with the samples from the first tantalum sputter deposition test. This caused some spalling of the coating on the grit-blasted

areas of the solid stainless steel specimens and minor, questionable spalling of the coating on the grit-blasted regions of the wire cloth specimens. However, the overall adhesion of the graphite coating to the grit-blasted areas of all the samples remained good.

As in the second sputter deposition test no significant grit-blasting pressure effect on the coating adhesion or spalling was observed in the graphite deposition test between comparable surface areas grit-blasted at the two pressures employed. This held true as well through the mechanical stressing and thermal cycling tests performed on the coated specimens.

D. Composite Target Sputter Deposition Test, Mission Equivalent

For the fourth sputter deposition test listed in table IV a composite sputtering target was employed having a composition by area of 46 percent carbon (pyrolytic graphite), 31 percent iron, 15 percent molybdenum, 6.7 percent stainless steel (type 304), and 1.7 percent tantalum. Figure 38 shows the target as prepared for the test. Sputtering of this target in the experimental configuration shown in figure 24 was judged to produce an approximately homogeneous flux of sputtered material depositing on the test samples. The desired weight composition of the sputter-deposited material was 54 percent iron, 35 percent molybdenum, 7.0 percent tantalum, 3.5 percent carbon, 0.3 percent chromium, and 0.1 percent nickel. This is the approximate average composition of sputtered material estimated to be depositing on the anode in an 8 cm diameter thruster currently undergoing a cycling life test, a test which is subsequently described in this paper. Apart from somewhat higher than desired chromium and nickel fractions arising from the exposed surface area of the stainless steel target holder, the target described was calculated to yield approximately the desired composition of sputtered material.

The composite target sputter deposition test was conducted with the same experimental arrangement and ion source conditions as previously

described, and the sputtering duration was the same as in the second and third tests. Thus the 2.3 to 3.5 μm thick sputtered coating deposited on the test specimens during the test is considered very roughly equivalent to that estimated to be produced on the anode in $\sim 10^4$ hours operation of the 8 cm thruster undergoing the cycling life test.

Operation of the ion source during the composite target sputter deposition test was halted overnight midway (2.25 hr) through the test, but the vacuum ($\sim 10^{-6}$ torr) was maintained during the shutdown. The purpose of this shutdown was to simulate one of the regular shutdown periods in the 8 cm thruster cycling life test. Of interest was whether such a shutdown could give rise to a discontinuity or layer indication in the sputter-deposited coatings due to oxidation or adsorption taking place under the vacuum conditions during the shutdown period. No evidence was seen in subsequent SEM examination of the coated specimens of any such effect.

The test samples exposed to sputter deposition in the composite target test were the same as those employed in the graphite sputtering test: solid stainless steel and the coarse and fine mesh stainless steel wire cloths, each grit-blasted at 14 and at 28 N cm^{-2} pressure. All the samples were pre-cut and mounted for the sputter deposition so that they could be directly examined with the SEM afterwards. The sputter-deposited coatings generated during the test appeared shiny and metallic for the most part, though irregular peripheral areas were evident which had a black appearance.

The sputtered coatings on the test specimens showed total adhesion, without cracks, flaws, or spalling, to the entire grit-blasted areas of the tested surfaces. The coating adhesion also was excellent to the nongrit-blasted regions of the fine mesh wire cloth specimens, with no spalling observed. On the coarse mesh wire cloth specimens, however, some spalling of the coating in flakes much less than a mesh unit long was noted from the nongrit-blasted areas, as seen in the SEM image shown in figure 39. (The same nongrit-blasted wire cloth surface was employed as the anode surface in the cycling life test subsequently described.) Spalling of the coating in large flakes was prominent on the nongrit-blasted regions of the solid specimens tested.

Under SEM examination, the top surface of the sputtered coatings
on the grit-blasted test sample surfaces showed good replication and
propagation of the original substrate surface features and appearance.
Typical is the SEM view in figure 40, showing at ×500 magnification
a coated boundary region between the grit-blasted and the nongrit-
blasted regions on the solid stainless steel specimen grit-blasted at
28 N cm^{-2}. On close examination under the SEM, the coating sur-
face on the grit-blasted regions generally showed evidence of slight
rounding and filling in of the original surface features and contours.
This effect, however, did not threaten to erase the original roughness
of the grit-blasted surface until a deposited coating at least several
times as thick as that actually observed in the test was built up.

Several types of nonuniform deposits were noted with the SEM
on coated sections of the test samples from the sputter deposition
test. Among these, nodular deposits found on the nongrit-blasted
areas of the fine mesh wire cloth samples were concentrated on the
steeply inclined, partially shielded sides of the wires deep within the
mesh openings. These deposits somewhat resembled the similarly
located deposits seen in figures 28(b) and 30(b).

On the coated grit-blasted surfaces of the fine mesh wire cloth
samples some microscopic lumpy deposits were observed with the
SEM. These created the slightly altered surface appearance seen
in figure 41 at ×700 magnification on the specimen grit-blasted at
14 N cm^{-2} pressure. Also noted in nonuniform distribution on both
the grit-blasted and the nongrit-blasted regions of all the test spec-
imens were small areas of a fine, densely packed, nodular and
vertical flake-like deposit. Both of these types of coating deposits
are believed to be anomalous, since they were not uniformly dis-
tributed over the sputter-coated sample areas. Their origin is un-
known but may again be related to factors such as the adhesive on
the polyimide tape used to shield the test specimens, as previously
suggested.

As in the second and third sputter deposition tests, no significant effect due to grit-blasting pressure was noted in the composite target test. The test specimen areas grit-blasted at 14 and at 28 N cm^{-2} pressure showed no appreciable difference in the appearance, adhesion, or other characteristics of their sputter-deposited coatings.

V.   EXTENDED THRUSTER TESTS OF GRAPHITE PARTS

One approach to remedying the sputter erosion of discharge chamber parts in mercury ion thrusters is to employ low sputter yield materials for the component surfaces most severely attacked. Graphite is an attractive material for use in fabricating these component surfaces because of its indicated low sputter yield to mercury ions. One extended test has been completed and another is currently being conducted to evaluate graphite discharge chamber parts during actual operation of small mercury ion thrusters. In both of these the graphite parts tested have been the baffle and the thruster backplate.

A.   400 Hour Test with Thick Baffle

The first extended test of a small thruster with a graphite baffle and backplate was an ~400 hour test (at 39.6 V ΔV_I) of a modified SIT-5 thruster equipped with an electrostatic vectoring grid assembly. The tested thruster was configured exactly as shown in figure 1 except for the use of a different baffle assembly and the absence of tantalum foil covers over the tip and outer flange surface of the cathode pole piece. Also, no anode insert was employed.

The baffle assembly used in the 400 hour test is shown before the test in figure 42, as mounted on the cathode pole piece. It consisted of a base piece and a mating, flush, top surface insert. Both parts were machined from anisotropic pyrolytic graphite oriented with the graphite atomic planes parallel to the flat surfaces of the structure. The baffle assembly was designed so that no material other than

graphite would be exposed to the thruster discharge downstream of the baffle support wire mount. The diameter of the graphite baffle assembly was 6.35 mm, the standard dimension for the SIT-5 baffle, but its thickness of 2.8 mm was much larger than the standard 0.63 mm thickness. The graphite baffle was mounted with its downstream surface flush with the cathode pole piece tip surface, as in the standard SIT-5 configuration.

The graphite backplate cover employed in the 400 hour test also was fabricated of anisotropic pyrolytic graphite (with the graphite atomic layers parallel to the flat surfaces). It was 0.53 mm thick.

The 400 hour test of the modified SIT-5 thruster with the above graphite parts was conducted continuously under the nearly standard SIT-5 conditions shown in table I. The actual duration of main discharge operation was 416 hours, with the high voltage on and beam extracted for 408 hours. The poor discharge utilization and consequently high accelerator drain current experienced during the test may be noted in table I. These characteristics were indicated in short operational tests with thin graphite baffles to be due principally to the excessive thickness of the baffle assembly.

After the 400 hour test, examination of the graphite baffle assembly showed very slight, general sputter erosion on the peripheral region of its downstream surface. On the exposed peripheral area of its upstream surface, however, a deposit was evident. Including only its graphite parts, the baffle assembly experienced a net weight gain of 8.1 mg during the test. This large relative weight gain sharply contrasted with the baffle weight losses found both in the ΔV_I erosion tests (ref. 4) and in the accelerated life test, described earlier. Basically the same thruster was employed in all these experiments, but a tantalum baffle was used both in the ΔV_I erosion tests and in the accelerated life test. The baffle weight loss in the accelerated life test was 25.6 mg, as shown in table II.

Low energy fluorescent X-ray analysis of the deposit found on the upstream surface of the graphite baffle assembly after the 400 hour

test established that the deposit consisted almost totally of mercury. (The presence also of some sputter-deposited carbon was likely but could not be confirmed since this element was undetectable by the X-ray analysis system used.) Nearly all of the weight gain experienced by the baffle assembly in the test was probably due to mercury sorbed by the graphite or present in the deposit described.

After the 400 hour test the pyrolytic graphite backplate cover showed slight, general sputter erosion of its exposed surface and also an indication of modest deposition of material (iron) sputtered from the outer edge of the cathode pole piece. This deposition on the backplate cover was in a narrow annular region immediately adjacent to the pole piece outer circumference. The cover was found to have suffered a net weight loss of 0.088 mg during the test. This is a factor of 40 to 80 less than the weight loss of the iron backplate in the most nearly comparable 400 hour ΔV_I erosion tests (ref. 4) with the same thruster. Again, mercury sorption by the graphite backplate cover is believed to be the principal reason for the almost negligible weight loss of the cover during the test.

The indicated sorption of mercury vapor by both the graphite baffle assembly and the graphite backplate cover during the 400 hour thruster test would contribute directly to the weight of each of these components at the end of the test and hence reduce or totally compensate any weight loss due to sputter erosion. Mercury sorption may also have had an even more important effect in directly reducing the sputter erosion of these parts during the test by generating a continuously renewing surface layer of adsorbed mercury. This adsorbed mercury layer would be sputtered in preference to the substrate and hence would protect the latter, at least partially, from sputtering damage.

The important effect of adsorbed mercury in reducing mercury ion sputtering of a substrate has been pointed out by G. S. Anderson. In his work on the mercury ion sputtering of nickel single crystal surfaces (ref. 14), Anderson provides evidence that mercury vapor ad-

sorption to form a complete monolayer occurs on such surfaces under experimental conditions very similar to those prevailing in an operating ion thruster. (These conditions include the presence of a low pressure mercury vapor discharge.) Such adsorption was strongly indicated to be responsible for the sharp reduction in Hg^+ ion sputtering of the nickel surfaces which Anderson observed at temperatures and pressures favoring the adsorption. The effect of mercury monolayer adsorption on ion thruster surfaces in reducing sputter erosion has not been conclusively established, but it warrants further investigation as a possible approach to solving the problems associated with sputtering in the discharge chamber.

The sputter-deposited coating built up on the anode interior surface during the 400 hour thruster test was insufficient to reliably indicate the adhesion, spalling tendency, or other characteristics of thicker coatings of like composition generated with graphite discharge chamber components in long-term thruster operation. No spalling or other flaws in the anode coating were noted.

After the 400 hour thruster test the pyrolytic graphite baffle assembly showed numerous incipient delaminations parallel to and presumably between its atomic layers. These threatened to cause the entire baffle assembly to split into separate pieces. Such a separation actually did occur with an identical baffle assembly which was initially employed in the 8 cm thruster cycling life test described subsequently. The anisotropic pyrolytic graphite of which both these baffle assemblies were fabricated is particularly susceptible to this type of structural failure because of its anisotropic thermal expansion properties and its weakness in the direction normal to the atomic layers. The relatively thin pyrolytic graphite backplate cover, which is subjected to less severe thermal gradients and stresses than is the baffle, did not exhibit any actual or incipient delamination after the 400 hour thruster test.

The thick baffle assembly made of anisotropic pyrolytic graphite thus demonstrated both a deleterious effect on thruster performance and a serious structural weakness. For both of these reasons it was

decided that a thin baffle employing an isotropic form of graphite was preferable. Such a revised baffle is shown in figure 43, as mounted on the SIT-5 cathode pole piece with a thin head tantalum screw. The dimensions of this baffle (6.35 mm diam by 0.63 mm thick), as well as the details of its mounting to the cathode pole piece, are essentially identical to those of the tantalum baffle employed in the accelerated life test (see fig. 1). The baffle was fabricated of a high purity isotropic grade of graphite having an apparent density of ~ 1.75 g cm^{-3}. (For comparison, the density of pyrolytic graphite approaches the 2.20 g cm^{-3} theoretical limit of graphite.) Five and 8 cm thrusters incorporating the thin design, isotropic graphite baffle, mounted as indicated in figure 1, have demonstrated satisfactory performance with no known baffle structural problems.

Neither the isotropic nor the anisotropic pyrolytic graphite thruster parts fabricated to date have been subjected to standard rocket launch vibration tests. Yet to be demonstrated is whether any type of graphite will show satisfactory fabrication and brittle fracture properties for general use in flight-qualified ion thruster parts. Despite the indicated superior sputter resistance of graphite in mercury ion thruster applications, tantalum may be the preferable material to fabricate sputter-resistant thruster parts of because of its much superior ductility and brittle fracture characteristics.

B. Cycling Life Test

A major extended life test of a laboratory 8 cm diameter mercury ion thruster equipped with a graphite baffle and backplate cover is currently in progress at the Lewis Research Center under the direction of S. Nakanishi. Details of the thruster construction, components, and operation through 7400 hours and 229 planned shutdowns and restarts have been described in reference 11. The thruster was initially equipped with a 0.53 mm thick pyrolytic graphite backplate cover and a 6.35 mm diameter by 2.8 mm thick pyrolytic graphite baffle assembly. The baffle assembly was identical to the one shown in figure 42,

which was employed in the 400 hour SIT-5 thruster test described in the previous section. After 1156 hours of thruster operation in the cycling life test the baffle assembly delaminated and split into two pieces, apparently for the reasons suggested earlier. It was therefore replaced with a thin baffle, identical to that shown in figure 43, made of isotropic, high purity (nonpyrolytic) graphite. The thin baffle, 6.35 mm in diameter by 0.63 mm thick, was mounted with a thin head tantalum screw in a manner similar to that shown in the figure.

Since the baffle replacement the thruster has continued to operate smoothly and restart easily. Through January, 1975, it had compiled a total of 9850 hours operation and 300 cycles, with no signs of imminent failure or of problems in the discharge operation. Typical operating conditions of the thruster after 9600 hours total running time are included in table I. As in the other thruster tests conducted with graphite baffles, relatively low discharge chamber utilization has been noted in the cycling life test.

The fractured pieces of the thick pyrolytic graphite baffle assembly removed after 1156 hours operation showed a net baffle weight gain of 48.6 mg in this period. Such a weight gain is consistent with the baffle weight gain observed in the 400 hour SIT-5 thruster test employing an identical baffle assembly. The pyrolytic graphite backplate cover used in the cycling life test, however, showed a large weight loss of 103.5 mg when weighed after 1156 hours of thruster operation. Such a large weight loss is inconsistent with the very small weight loss of the same type backplate cover in the 400 hour SIT-5 thruster test. The disagreement may be attributable to the several differences between the 5 and 8 cm thrusters employed, particularly in size and in the presence of an auxiliary high voltage cathode starting electrode in the latter.

The anode employed in the SIT-8 thruster undergoing the cycling life test is equipped with an interior surface fabricated of coarse mesh stainless steel wire cloth. This wire cloth, described in the footnotes of table IV, is the same as the coarse mesh wire cloth tested in the

experiments reported in foregoing sections of this paper. The anode surface was not grit-blasted for the cycling life test due to initiation of the test prior to the grit-blasting investigations reported herein. When weighed after 1156 hours operation in the life test, the anode showed a weight gain of 57.9 mg. It also showed no actual or incipient spalling of the sputter-deposited coating on its interior surface. The expected average composition of this coating has been described previously in the discussion of the composite target sputter deposition test, in which efforts were made to achieve the same sputtered material composition.

The continued smooth operation of the 8 cm thruster in the cycling life test after 9850 hours indicates no critical sputter erosion of any discharge chamber component has taken place. It also indicates that no significant spalling of the sputter-deposited anode coating has occurred, a conclusion supported by direct telescopic observation of the anode surface.

VI. CONCLUSIONS

This paper has described the results of an accelerated thruster life test, four sputter deposition tests of candidate anode surfaces, and two extended thruster tests with graphite parts. Together with the previously reported conclusions from sputter erosion tests conducted as a function of discharge potential (ΔV_I), these results suggest four possible approaches to solving the problems of discharge chamber sputtering and anode deposit spalling in small mercury ion thrusters. These are summarized below.

1. Fabricate sputtered discharge chamber component surfaces from materials with superior resistance to low energy mercury ion sputtering. Tantalum and graphite are two such materials which have demonstrated excellent sputter resistance in the reported and in other thruster experiments.

2. Fabricate the anode interior surface, which is the predominant site for deposition of sputtered material in the thruster, of a fine mesh wire cloth and carefully prepare this surface for maximum adhesion

of the sputter-deposited coating which builds up on it. The purpose of the wire cloth is to limit the size of any coating flakes which might spall from it to dimensions which are innocuous in the thruster. In the experiments here reported, fine mesh wire cloth surfaces made of 0.045 to 0.050 mm stainless steel wire have been found effective in thus limiting the flake size of spalled coatings up to perhaps 30 μm thick (~60 percent of the wire diameter). Coarse grit-blasting of the anode surface to produce maximum surface feature roughness is the anode surface to produce maximum surface roughness is the blasting prescription has been developed (table III). In the experiments here reported stainless steel surfaces grit-blasted by the optimized procedure, and in particular the fine mesh wire cloth surfaces so prepared, have demonstrated outstanding adhesion for representative sputtered coatings up to 30 μm thick, even on moderate mechanical stressing and thermal cycling. The surface features of the grit-blasted substrate, which are typically 10 μm in size for the optimally prepared surface, are accurately replicated and preserved through sputtered coatings at least three times this dimension in thickness. This characteristic apparently contributes to the excellent sputtered coating adhesion observed, even of thick coatings, to the grit-blasted surfaces and to previously deposited layers of the coatings themselves.

3. Promote mercury vapor adsorption on the discharge chamber surfaces subject to intense sputtering. The experiments conducted with graphite baffles and thruster backplates suggest that such adsorbed mercury contributes significantly to protecting the substrate surfaces from sputter erosion.

4. Operate the thruster at as low a ΔV_I as feasible and actively control the ΔV_I within narrow limits. If the thruster is operated so that the primary electron energy in the main discharge is in the range of ~19 to 28 eV, lowering this energy by lowering ΔV_I is very effective in reducing the discharge chamber sputtering rates. The reduced sputtering results from the corresponding substantial decrease

in the production of the doubly charged mercury ions principally responsible for the sputtering damage.

Implementation of these approaches can apparently eliminate discharge chamber sputtering, sputtered material deposition, and sputtered deposit spalling as life-limiting processes in small mercury ion thrusters. Among the described tests providing a demonstration of this is an ongoing cycling life test of an 8-cm diameter thruster employing a graphite baffle and backplate cover, together with a coarse wire cloth anode surface. This test shows no sign of discharge chamber sputtering problems after 10 000 hours of thruster operation. Utilizing the approaches suggested should make possible 20 000 or more hours of reliable small thruster operation free of problems arising from internal sputtering.

REFERENCES

1. Hudson, W. R., and Banks, B. A., "An 8-Centimeter Electron Bombardment Ion Thruster for Auxiliary Propulsion," AIAA Paper 73-1131, Lake Tahoe, Nev., 1973.

2. Nakanishi, S., and Finke, R. C., "A 9700-Hour Durability Test of a Five Centimeter Diameter Ion Thruster," AIAA Paper 73-1111, Lake Tahoe, Nev., 1973.

3. Mantenieks, M. A., and Rawlin, V. K., "Studies of Internal Sputtering in a 30-Cm Thruster," AIAA Paper 75-400, New Orleans, La., 1975.

4. Power, J. L., "Sputter Erosion and Deposition in the Discharge Chamber of a Small Mercury Ion Thruster," AIAA Paper 73-1109, Lake Tahoe, Nev., 1973.

5. Hyman, J., Jr., "Performance Optimized, Small Structurally Integrated Ion Thruster System," May 1973, Hughes Research Labs., Malibu, Cal.; also CR-121183, 1973, NASA.

6. Power, John L.: Accelerated Life Test of Sputtering and Anode Deposit Spalling in a Small Mercury Ion Thruster. NASA TM in

preparation, 1975.

7. Industrial Airbrasive Unit, Model F, manufactured by S. S. White Co. (Abrasive powders used also manufactured by S. S. White Co.)

8. "Metal Progress Databook," vol. 104, no. 1, June 1973.

9. "Metals Handbook," 8th ed., vol. 1 (American Society for Metals, Novelty, Ohio, 1961).

10. "1972 Materials Selector," Materials Engineering, Vol. 74, No. 4, Mid-Sept. 1971.

11. "8-Centimeter Mercury Ion Thruster System Technology," AIAA Paper 74-1116, San Diego, Cal., 1974.

12. Moore, A. W., "Highly Oriented Pyrolytic Graphite," Chemistry and Physics of Carbon, vol. 11, 1973, pp. 69-187.

13. Carter, G.; and Colligon, J. S.: Ion Bombardment of Solids. (American Elsevier, New York, 1968), p. 323.

14. Anderson, G. S., "Hg Adsorption Studies Using Atom Ejection Patterns," Journal of Applied Physics, Vol. 36, No. 5, May 1965, pp. 1558-1561.

TABLE I. - CHARACTERISTIC OPERATING CONDITIONS

DURING THRUSTER TESTS

Thruster diameter, cm	5	5	8
Test characterization	accel. life test	graphite parts test	cycling life test
Baffle material	Ta	C	C
Length of test[a], hr	200	[b]408	[c]9600
Discharge potential, ΔV_I, V	64.6	39.6	40.0
Ion beam accelerating potential[d], $V_I + V_G$, V	1393	1397	1225
Accelerator potential, V_A, V	-700	-700	-500
Beam current, J_B, mA	23.4	23.4	72.0
Accelerator drain current, J_A, mA	0.063	0.171	0.22
Emission current, J_E, mA	372	228	710
Cathode Hg flow rate[e], $\dot{m}_C$, equiv. mA	29.9	46.7	116
Cathode keeper potential, V_{CK}, V	15	14	15.5
Cathode keeper current, J_{CK}, mA	400	400	200
Cathode tip heater power, W	0	0	0
Discharge propellant utilization[f], percent	78.2	50.1	62.1
Discharge losses[g], eV/ion	1027	386	394

[a]Time of beam extraction.

[b]Main discharge on 416 hr.

[c]Test ongoing; operating conditions listed as of 9600 hr operation; time of operation through Jan. 1975: 9850 hr.

[d]Equals net accelerating potential, V_I, plus neutralizer coupling potential, V_G (<0).

[e]Includes all main discharge mercury flow.

[f]Neglecting double ionization.

[g]Excluding cathode keeper losses and neglecting double ionization.

TABLE II. - MAJOR COMPONENT WEIGHT LOSSES IN

ACCELERATED LIFE TEST

Component	Initial weight, g	Weight loss, mg
Cathode pole piece[a]	10.9	11.4
Cathode pole piece tip cover	0.182	59.5
Cathode pole piece outer flange cover	0.561	14.5
Baffle	0.267	25.6
Baffle screw	0.110	8.8
Baffle nut and washer[b]	0.159	1.4
Backplate cover	16.2	5.4
Screen grid upstream surface[c]	-----	[d]90.1

[a]With baffle parts and tantalum covers disassembled.

[b]Located upstream of baffle location; see fig. 1.

[c]All screen grid erosion observed to be on upstream surface.

[d]Estimated from total measured grid system weight loss of 99.5 mg.

TABLE III. - OPTIMIZED GRIT-BLASTING VARIABLES

Variable	Range investigated	Optimized value
Grit material	SiC, Al_2O_3	SiC
Particle size, μm	SiC: 25, 50; Al_2O_3: 27, 50	50
Grit-blasting time, sec	2 to 60	12
Distance[a], cm	0.63 to 2.5	2.5
Nozzle orifice size, mm	0.28 to 0.71	0.46
Pressure, N cm^{-2}	14 to 55	28
(psi)	(20 to 80)	(40)
Feed rate[b], mg min^{-1}	[c]100 to 1400	[d]350
Angle of attack, deg	45, 90	90

[a]Nozzle to specimen.

[b]Approximate values only - controlled by vibrator voltage in S. S. White Co. "Airbrasive" unit employed. See text.

[c]Vibrator voltage range, 30 to 90 V.

[d]Vibrator voltage setting, 60 V.

TABLE IV. - SPUTTER DEPOSITION TESTS ON OPTIMALLY

GRIT-BLASTED SURFACES

Test number	1	2	3	4
Deposition surfaces:				
Fine cloth[a]	Yes	Yes	Yes	Yes
Coarse cloth[b]	Yes	No	Yes	Yes
Solid stainless steel	Yes	Yes	Yes	Yes
Solid Ta	Yes	Yes	No	No
Grit-blasting pressures[c], N cm^{-2}	14	14	14	14
	28	28	28	28
	55			
Beam-on time[d], hr	30	[e]4.5	4.5	[f]4.5
Target material	Ta	Ta	[g]C	[h]Composite
Sputtered coating thickness, μm	[i]18 to 29	2.3	1.0	[j]2.3 to 3.5
Equivalent small thruster operating time[k], hr	[l]~1×10^5	~1×10^4	~1×10^4	~1×10^4
Mechanically stressed[m]	Yes	No	Yes	No
Thermally cycled[n]	Yes	No	Yes	No

[a]Fine stainless steel wire cloth: double woven, 80 × 450 wires/cm, 0.045 to 0.050 mm diam wire.

[b]Coarse stainless steel wire cloth: double woven, 20 × 100 wires/cm, 0.20 to 0.25 mm diam wire.

[c]Grit-blasted test samples prepared at all indicated pressures for all indicated deposition surfaces. Except for the pressure, the optimized grit-blasting prescription of table III was employed for all samples.

[d]Of 8 cm diam mercury ion thruster used as sputtering ion source.

[e]Beam on 30 sec, then stopped; deposition surfaces exposed to atmosphere, then test completed. See text.

[f]Beam on 2.25 hr, then stopped; deposition surfaces maintained overnight under vacuum, then test completed. See text.

[g]Pyrolytic (anisotropic) graphite.

[h]Target composition by area: C (pyrolytic graphite), 46 percent; Fe, 31 percent; Mo, 15 percent; type 304 stainless steel, 6.7 percent; Ta, 1.7 percent. See text.

[i]Average thicknesses on individual deposition surfaces: fine mesh wire cloth, 28.5 μm; coarse mesh wire cloth, 26.2 μm; solid stainless steel, 17.7 μm; and solid Ta, 29.1 μm.

[j]Average thicknesses on individual deposition surfaces: coarse mesh wire cloth, 3.5 μm; solid stainless steel, 2.3 μm.

[k]See text.

[l]For average sputtered coating thickness of 25 μm.

[m]Procedure: bend specimen tightly around 0.64 cm diam rod with coated surface on outside, then straighten specimen back to flat condition; repeat procedure.

[n]Procedure: heat specimen in air to 250° C; hold at this temperature for 1 hr; allow to cool to room temperature; hold at room temperature for 20 min; repeat whole procedure two more times.
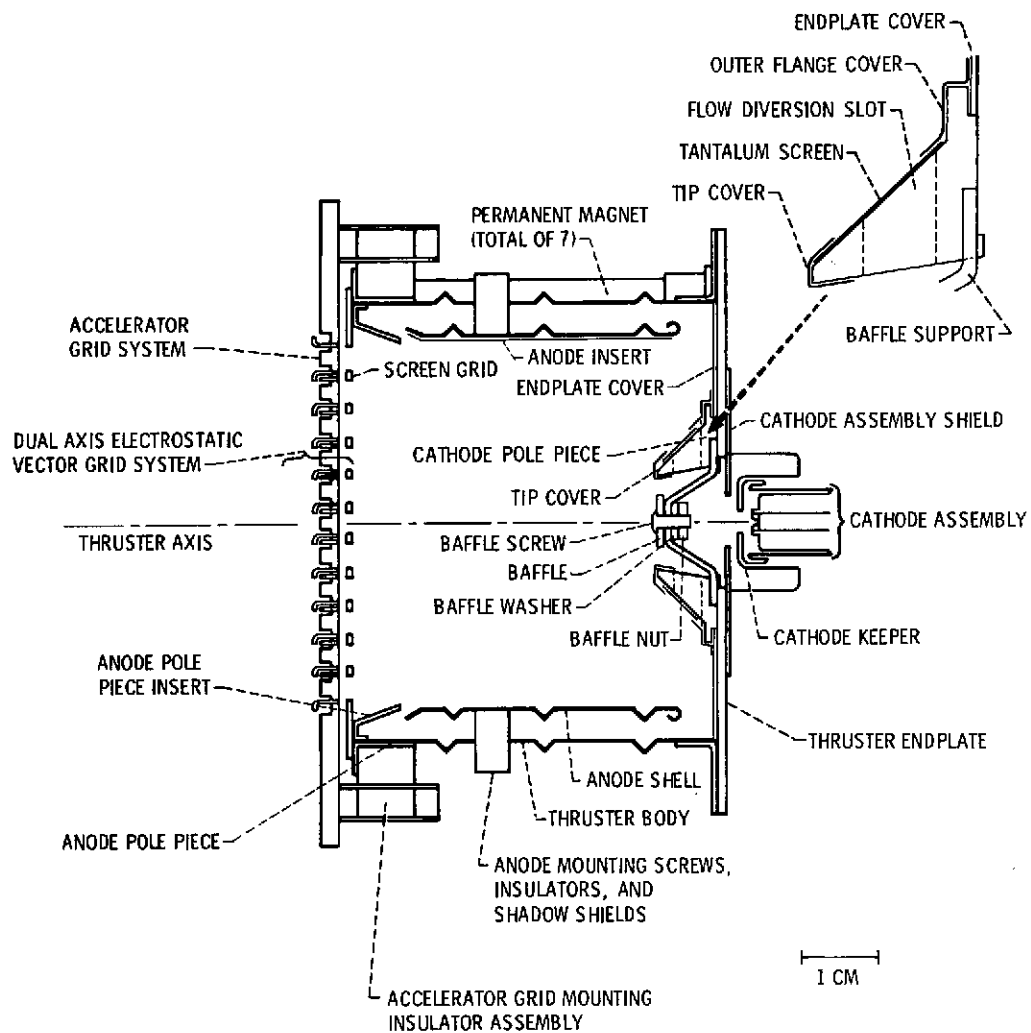
Figure 1. - Sectional view of modified 5-cm thruster used in accelerated life test. Neutralizer and ground screen not shown.
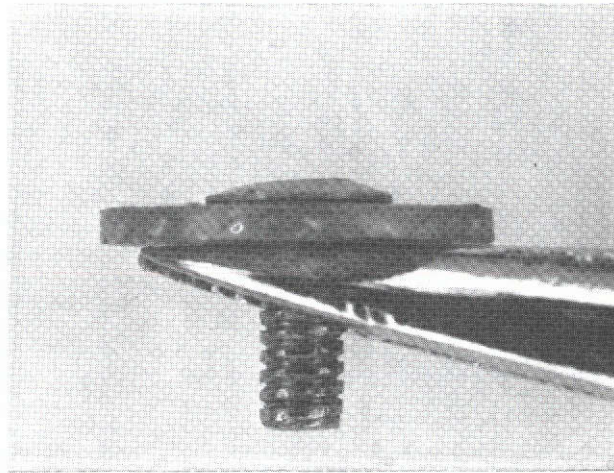
Figure 2. - Tantalum baffle and baffle screw, before test.
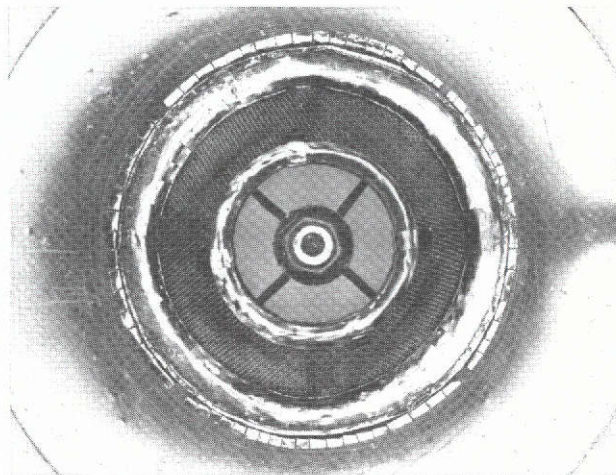
Figure 3. - Cathode pole piece-baffle assembly with tantalum foil covers, before test.
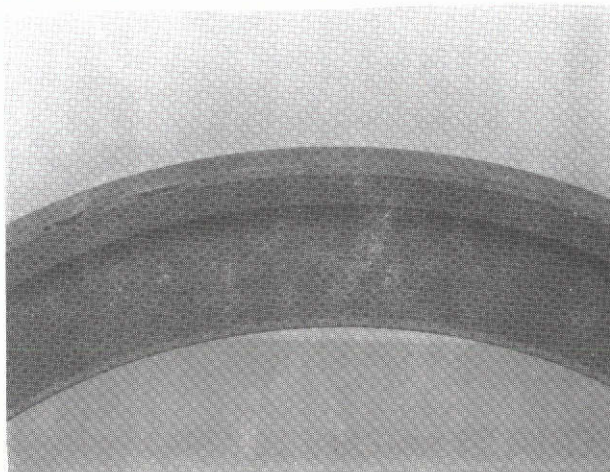
Figure 4. - Upstream side of anode pole piece insert, before test, showing tantalum plasma-sprayed interior surfaces.
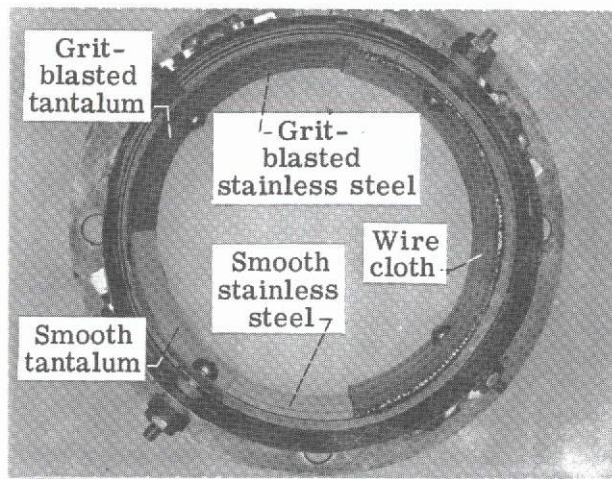
Figure 5. - Composite anode assembly, before test, looking upstream.
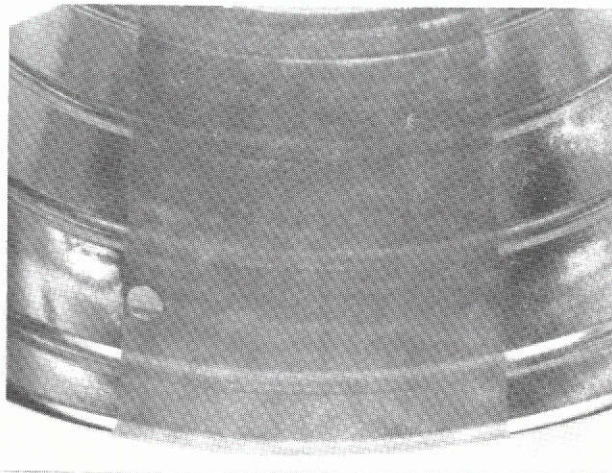
Figure 6. - Grit-blasted and virgin stainless steel anode shell surfaces, before test.
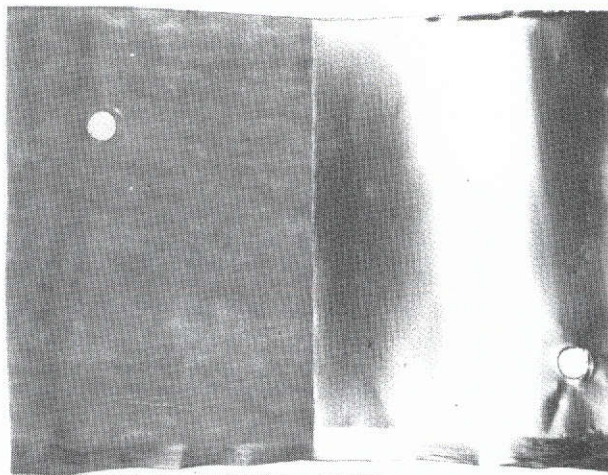
Figure 7. - Grit-blasted (left) and smooth (right) tantalum foil anode insert surfaces, before test.

1 mm
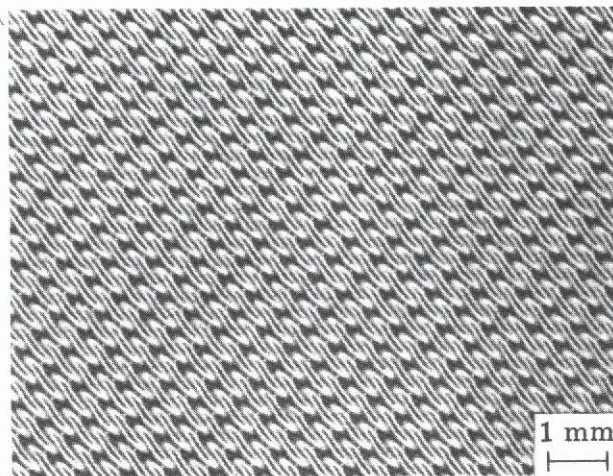
Figure 8. - Stainless steel wire cloth anode insert surface, before test.
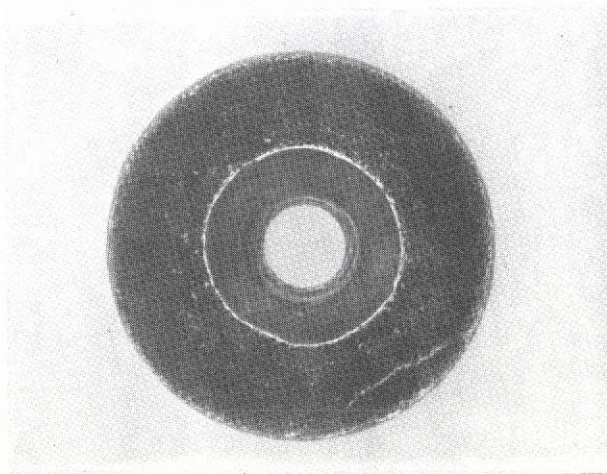
Figure 9. - Downstream surface of baffle, after test. Central area covered by baffle screw head. (Test conducted for 200 hr at $\Delta V_I = 64.6$ V.)
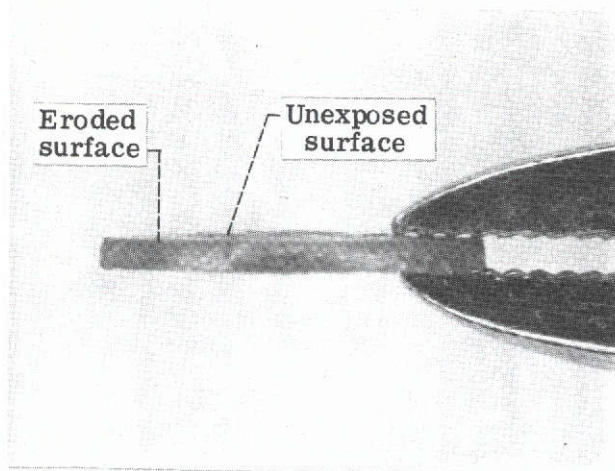
Figure 10. - Edge view of baffle, after test. Downstream surface up.
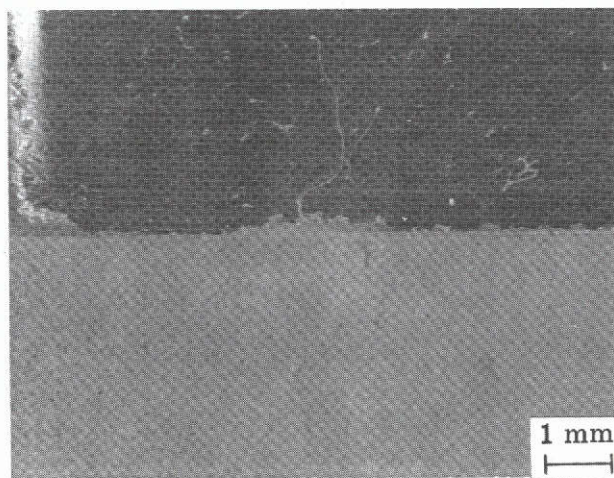
Figure 11. - Portion of tantalum foil anode insert, after test, showing coated grit-blasted surface, at bottom, and smooth surface with coating spalled off, at top.
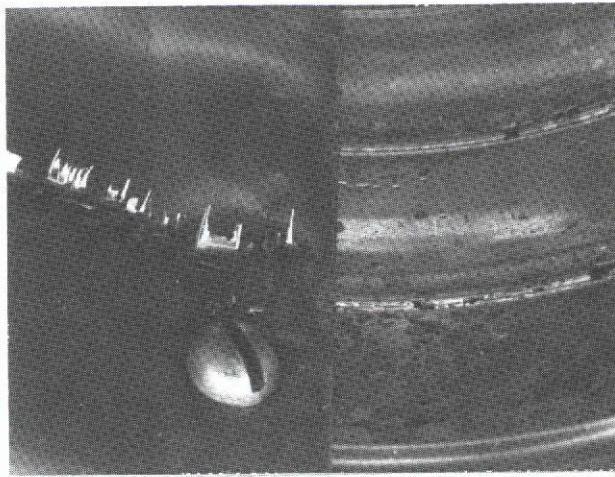
Figure 12. - Interior view of anode surface after test. Smooth tantalum foil insert surface at left; smooth stainless steel shell surface at right.

0.10 mm
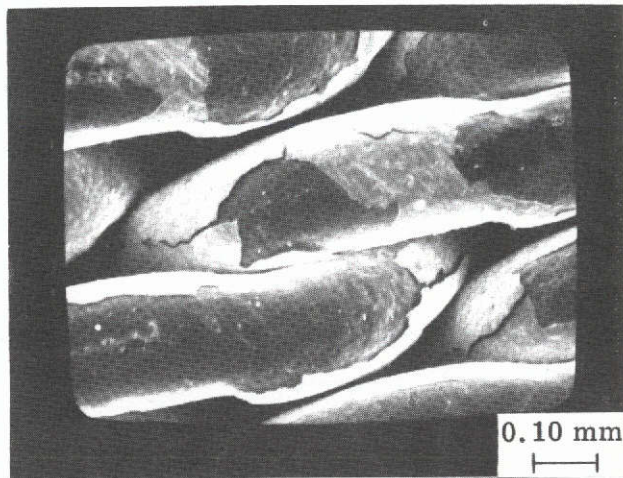
Figure 13. - Spalled coating on stainless steel wire cloth anode insert, after test.
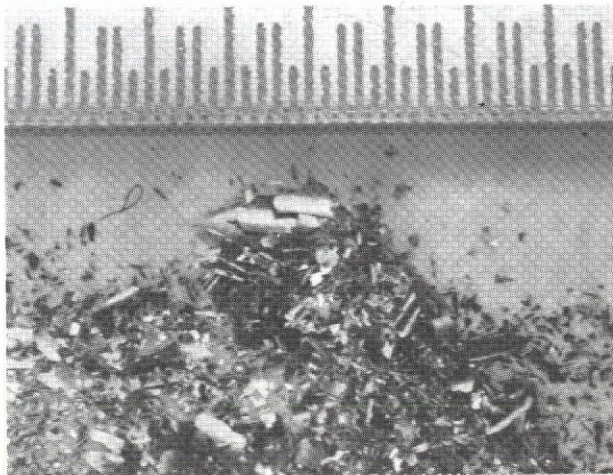
Figure 14. - Portion of loose flakes and material collected from thruster discharge chamber after test. Smallest intervals on ruler each 0.254 mm (0.01 in.).
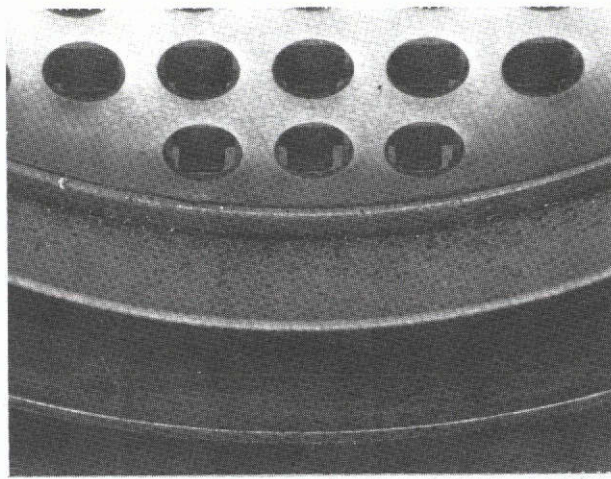
Figure 15. – Loose flakes on interior surface of anode pole piece insert, after test.

50 μm
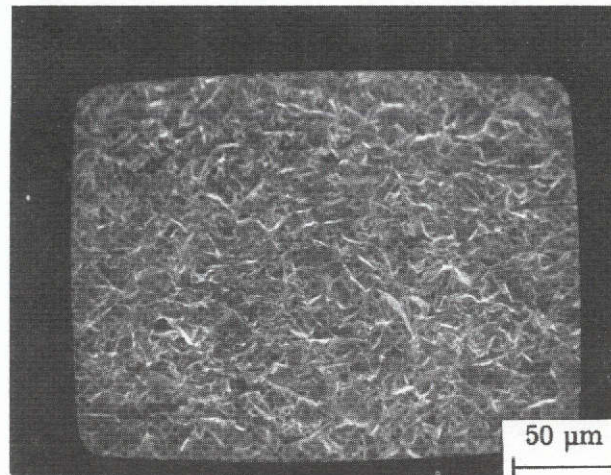
Figure 16. – Solid stainless steel, coarsely grit-blasted. SEM conditions: 700 X, 60° tilt.

50 μm
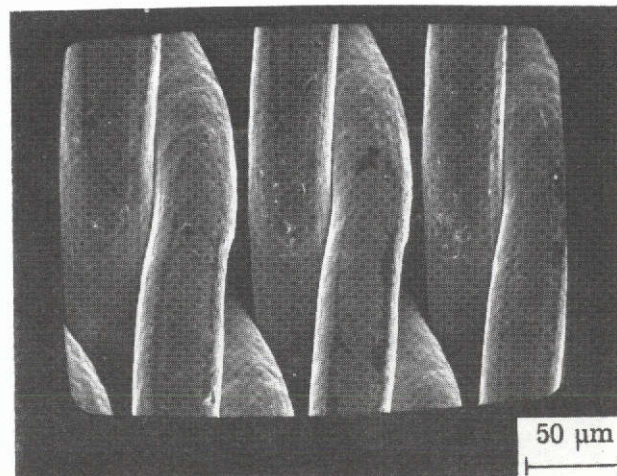
Figure 17. – Fine mesh, double woven stainless steel wire cloth. SEM conditions: 700 X, 0° tilt.
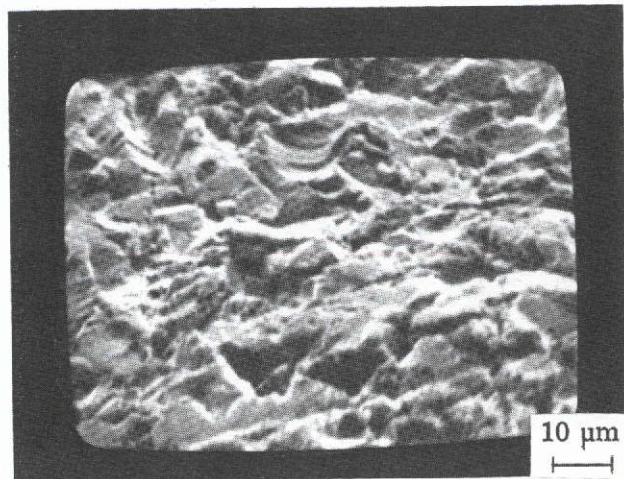
(A) Grit-blasting abrasive: 50 μm SiC.
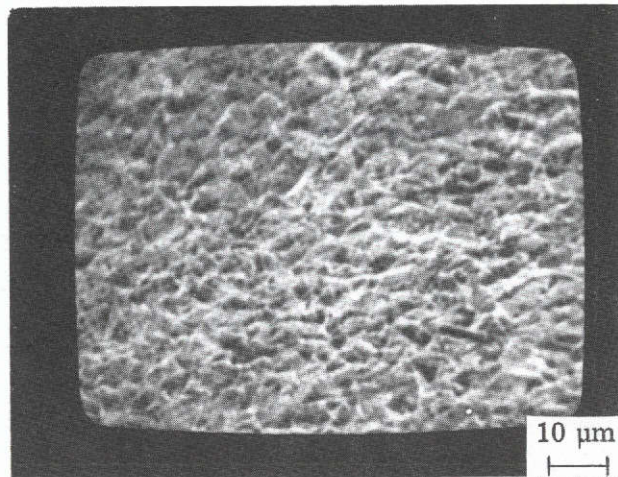
(B) Grit-blasting abrasive: 25 μm SiC.

Figure 18. – Solid stainless steel, grit-blasted
30 sec. SEM conditions: 2000 X, 60º tilt.
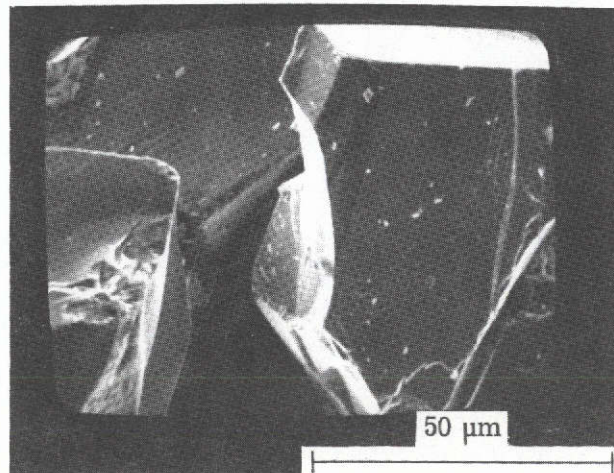
Figure 19. – 50 μm silicon carbide abra-
sive powder. SEM conditions: 2000 X,
0º tilt.
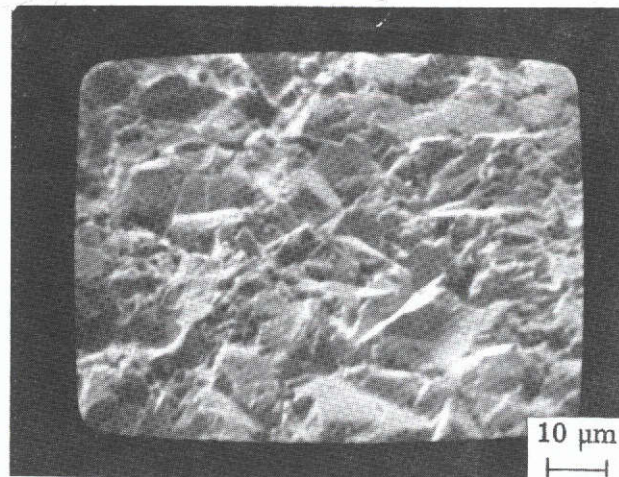
(A) Stainless steel.
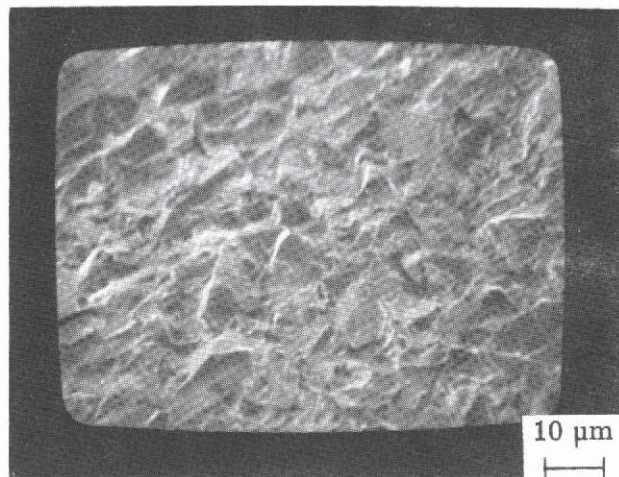
(B) Molybdenum.

Figure 20. - Solid materials comparatively
  grit-blasted (12 sec). SEM conditions: 2000
  X, 60° tilt.

10 µm
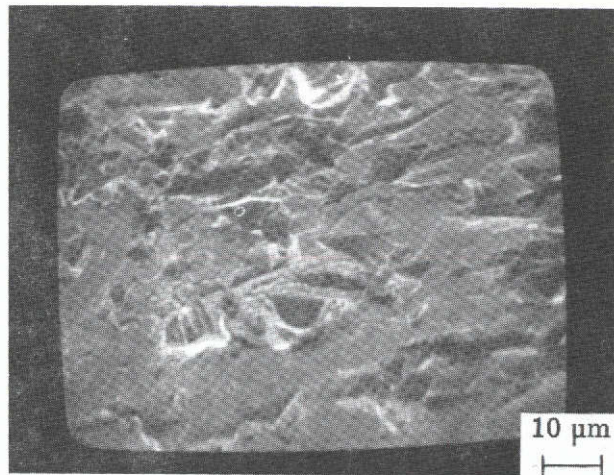
(A) 2 sec grit-blasting time.

10 µm
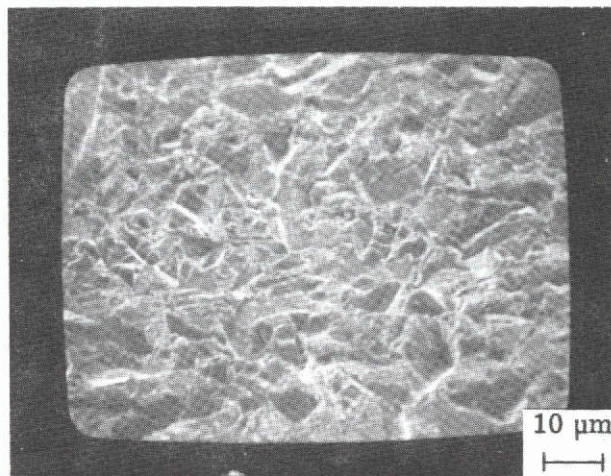
(B) 12 sec grit-blasting time.

Figure 21. - Solid stainless steel comparatively
grit-blasted for different times under other-
wise optimized conditions. SEM conditions:
2000 X, 60° tilt.

10 µm
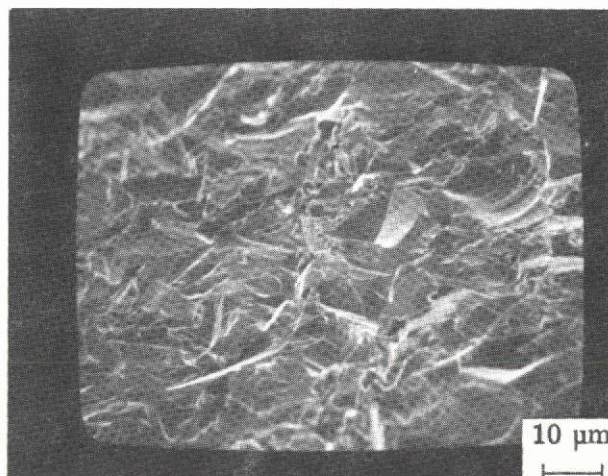
Figure 22. - Solid stainless steel grit-
blasted at 45° angle of attack. SEM con-
ditions: 2000 X, 60° tilt.
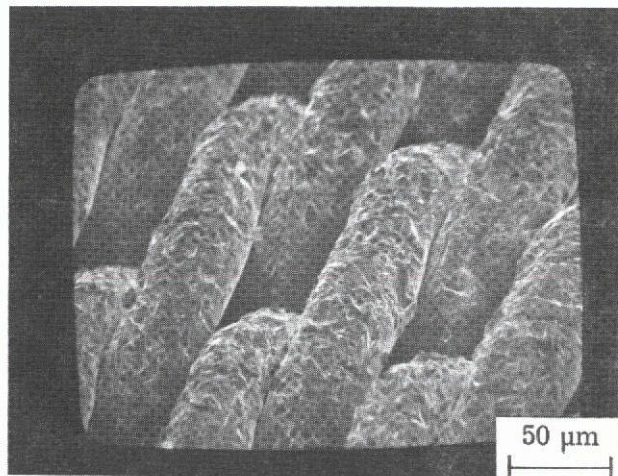
(A) 14 N cm^{-2} grit-blasting pressure.
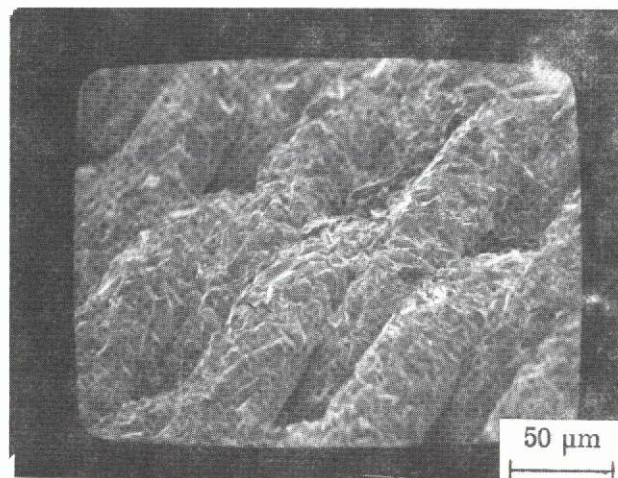
(B) 28 N cm^{-2} grit-blasting pressure.
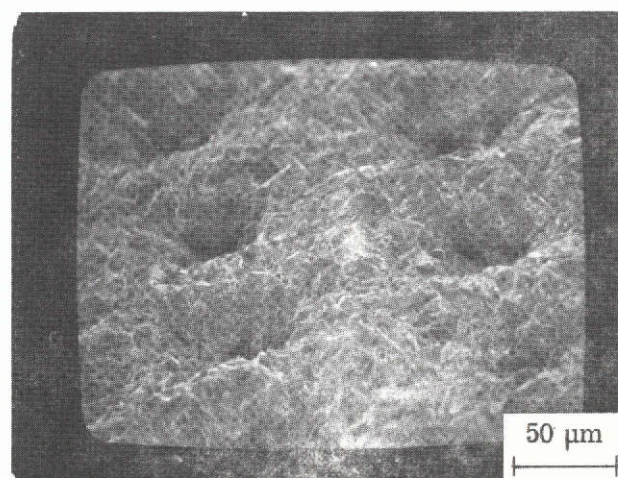
(C) 41 N cm^{-2} grit-blasting pressure.

Figure 23. - Fine mesh stainless steel wire cloth, comparatively grit-blasted at different pressures under otherwise optimized conditions. SEM conditions: 700 X, 60° tilt.

MOUNTING
BRACKETS
(2.5 CM WIDE)

ION EXTRACTION GRID
SYSTEM OF 8 CM THRUSTER

₵

TEST DEPOSITION SURFACE
MOUNTING BLOCK

10.2 CM

SPUTTERED EFFLUX
FROM TARGET

5.3 CM

25.4 CM

8.0 CM
DIAM

7.2 CM

₵

ION BEAM

45°

TARGET
(6.2 CM WIDE)

TARGET AND TEST DEPOSITION SURFACES
MOUNTED AT THRUSTER MIDPLANE ELEVATION

AREA OF TARGET
MOUNTING BRACKET
EXPOSED TO ION
BEAM CONSIDERED
PART OF TARGET

SCALE

10 CM
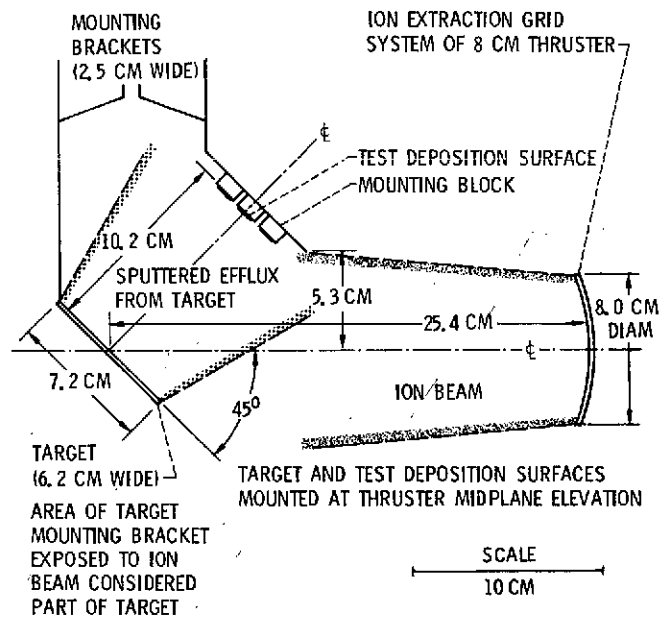
Figure 24. - Experimental configuration for sputter deposition tests.
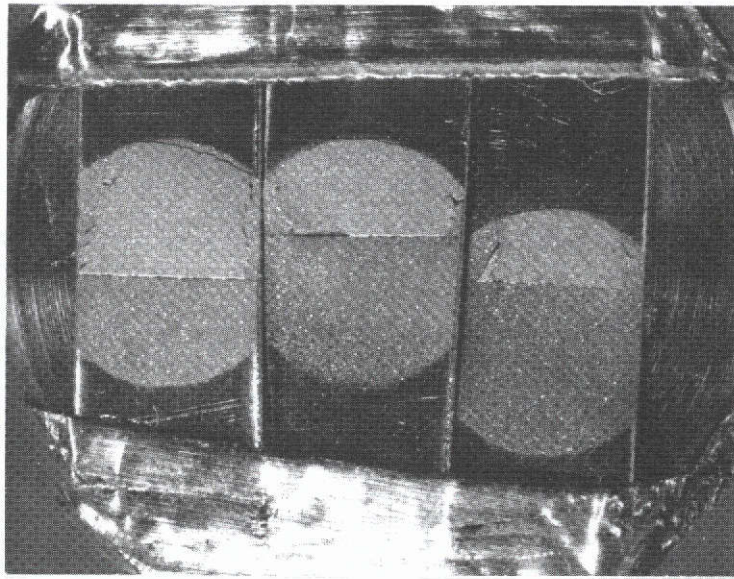
(A) As prepared for SEM examination.
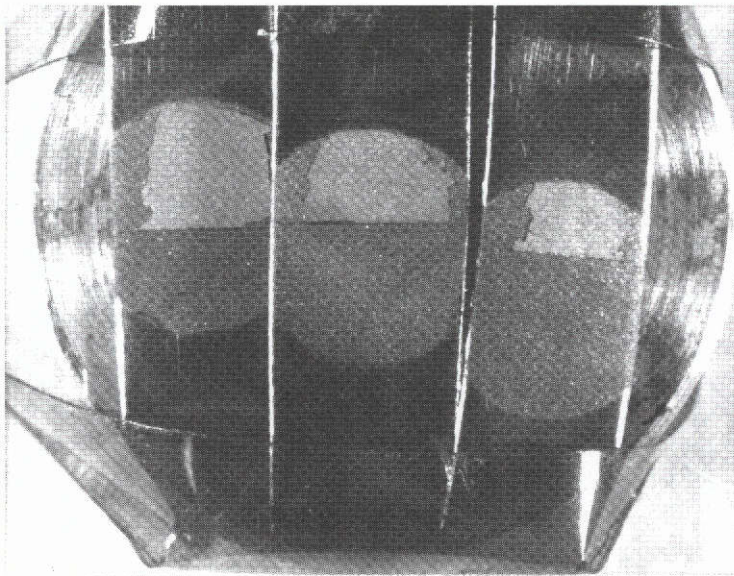
(B) After mechanical stressing and thermal cycling.

Figure 25. - Solid stainless steel specimens after thick tantalum sputter deposition test. (Equivalent to $\sim 10^5$ hr small thruster operation.) Areas grit-blasted at 14 (left), 28 (center), and 55 (right) $N\ cm^{-2}$ pressure.
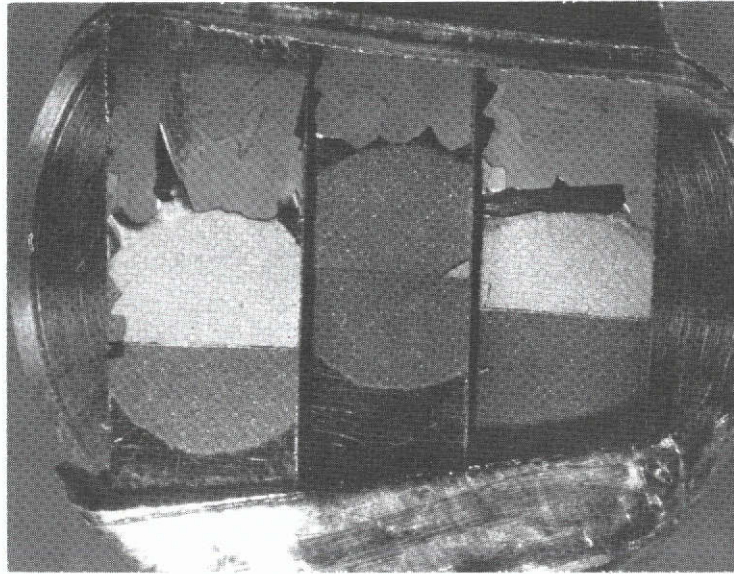
(A) As prepared for SEM examination.
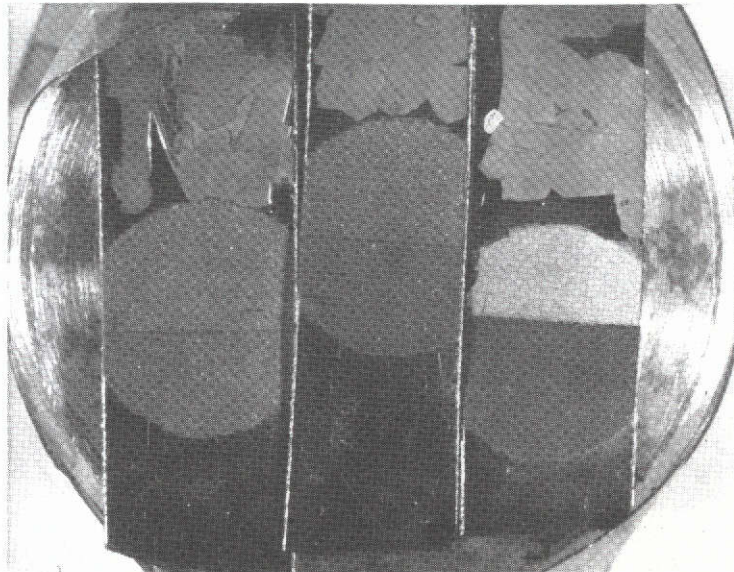
(B) After mechanical stressing and thermal cycling.

Figure 26. - Solid tantalum specimens after thick tantal-
um sputter deposition test. Areas grit-blasted at 14
(left), 28 (center), and 55 (right) N cm^{-2} pressure.
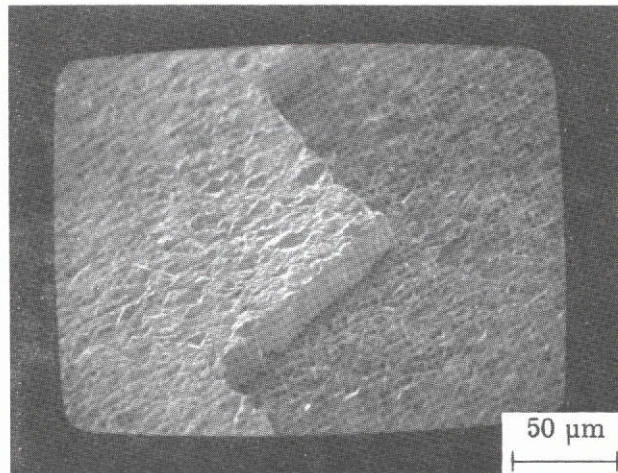
(A) Grit-blasting pressure 14 N cm^{-2}.
SEM conditions: 700 X, 60° tilt.
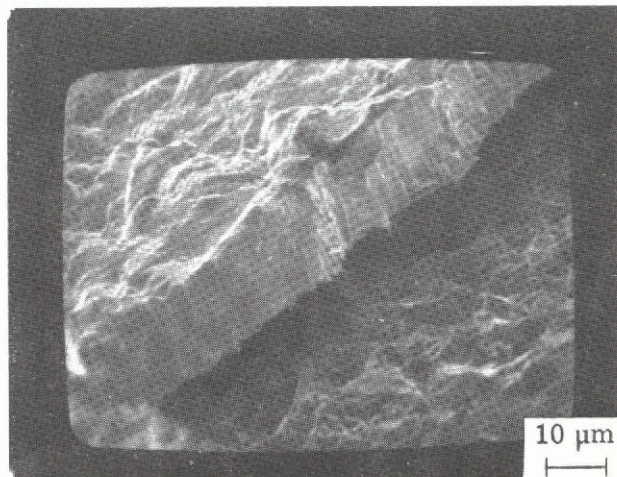
(B) Grit-blasting pressure 28 N cm^{-2}.
SEM conditions: 2000 X, 60° tilt.

Figure 27. - Broken edges of thick sputtered
tantalum coating on grit-blasted solid stain-
less steel specimens, showing replication of
grit-blasting features in coating surface.
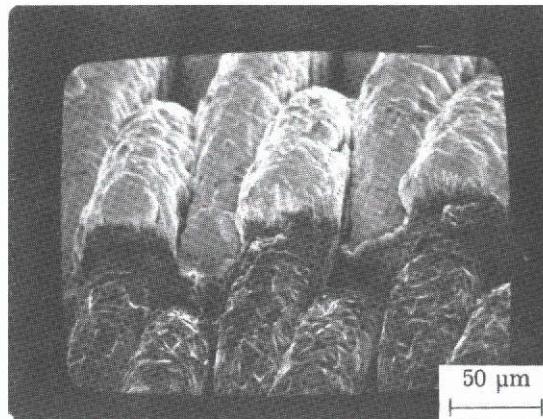
(A) Boundary between coated and non-coated areas.
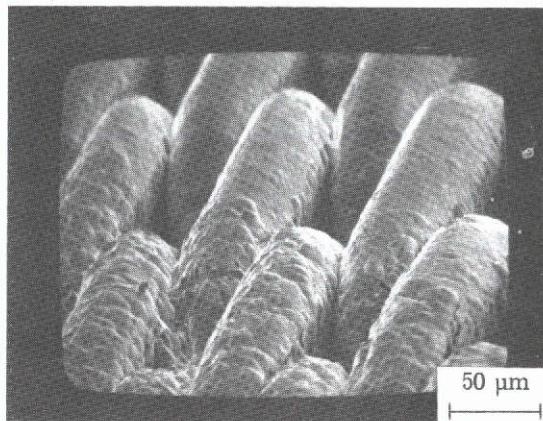
(B) Coated area across boundary between grit-blasted and non-grit-blasted regions.

Figure 28. - Thick sputtered tantalum coating on fine mesh stainless steel wire cloth grit-blasted at 14 N cm^{-2}, showing replication of grit-blasting features in coating surface. SEM conditions: 700 X, 60° tilt.
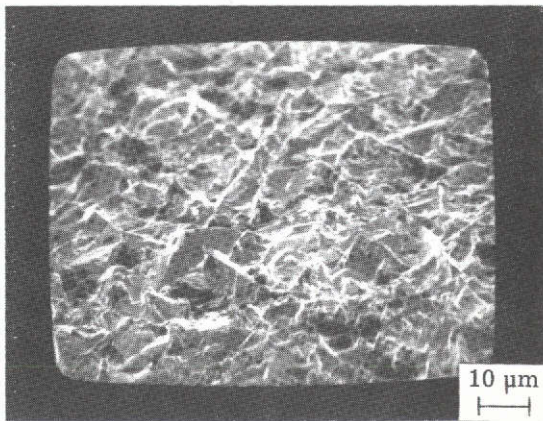
Figure 29. - Under surface of thick sputtered tantalum coating flake spalled from solid tantalum specimen grit-blasted at 14 N cm^{-2}. SEM conditions: 2000 X, 60° tilt.
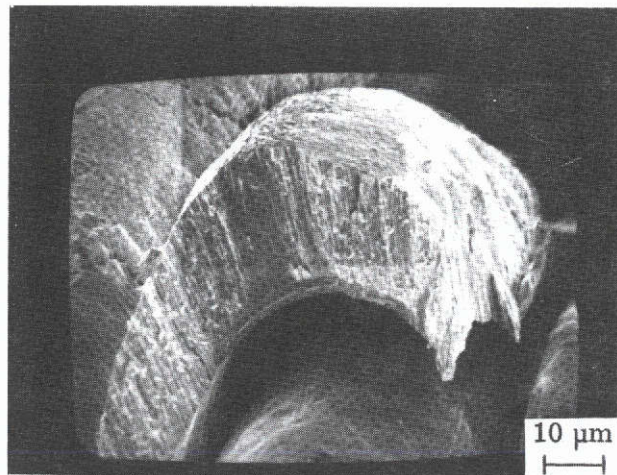
(A) Broken coating edge.
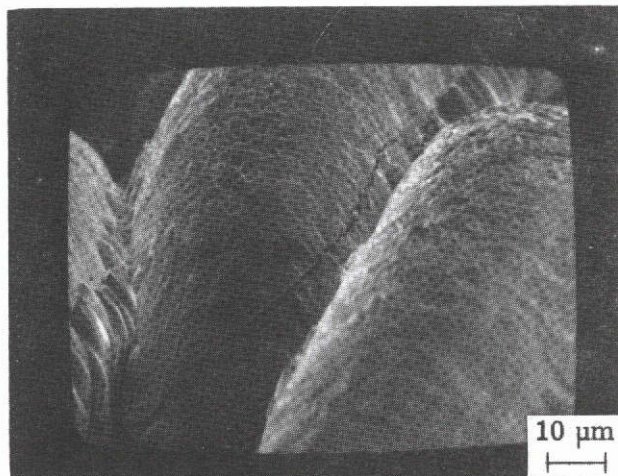
(B) Cracked coating surface.

Figure 30. - Thick sputtered tantalum coating
on non-grit-blasted areas of fine mesh stain-
less steel wire cloth. SEM conditions:
2000 X, 60° tilt.
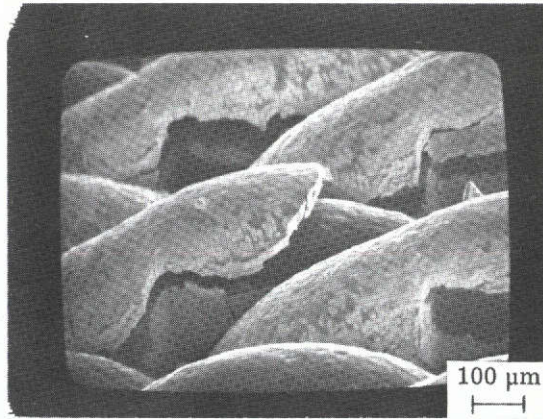
Figure 31. - Thick sputtered tantalum coat-
ing spalled from non-grit-blasted area of
coarse mesh stainless steel wire cloth.
SEM conditions: 200 X, 60° tilt.
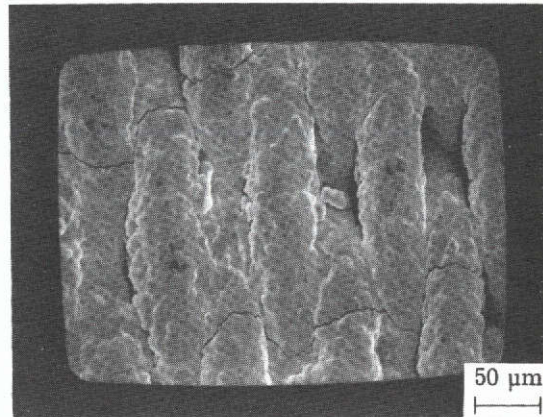
Figure 32. - Cracks in thick sputtered tan-
talum coating on fine mesh stainless
steel wire cloth grit-blasted at 28 N cm^{-2},
after mechanical stressing. SEM condi-
tions: 500 X, 0° tilt.
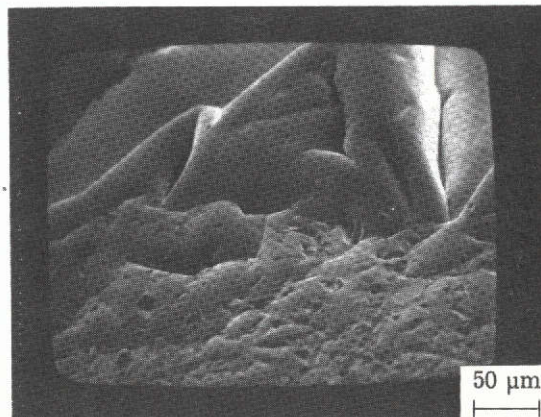
Figure 33. - Thin sputtered tantalum coat-
ing (equivalent to coating from ~10^4 hr
small thruster operation) on solid tan-
talum specimen grit-blasted at 28 N
cm^{-2}, showing coated area across bound-
ary between grit-blasted region (fore-
ground) and non-grit-blasted region
(background). Note spalling of coating
to boundary. SEM conditions: 500 X,
60° tilt.
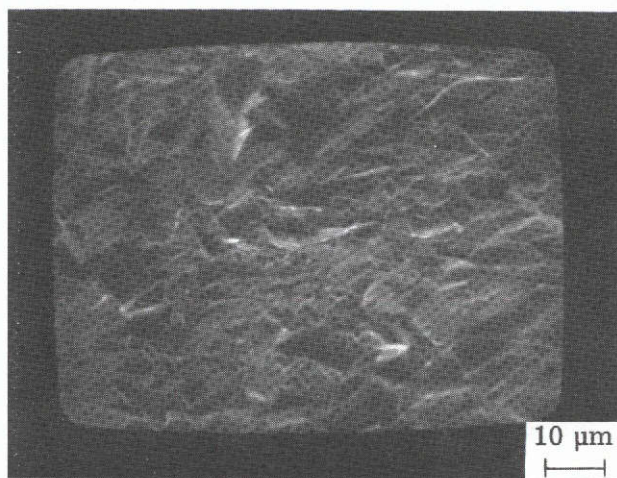
(A) Non-coated area.
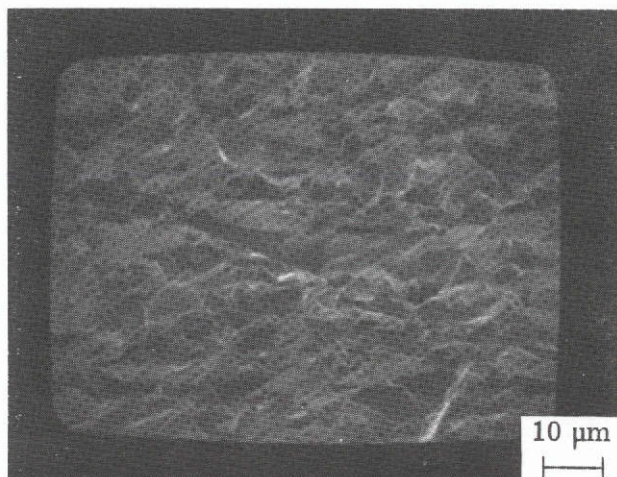
(B) Coated area.   Note similarity to non-
coated area.

Figure 34. - Solid stainless steel specimen
grit-blasted at 28 N cm^{-2} for thin tantalum
sputter deposition test. SEM conditions:
2000 X, 60° tilt.
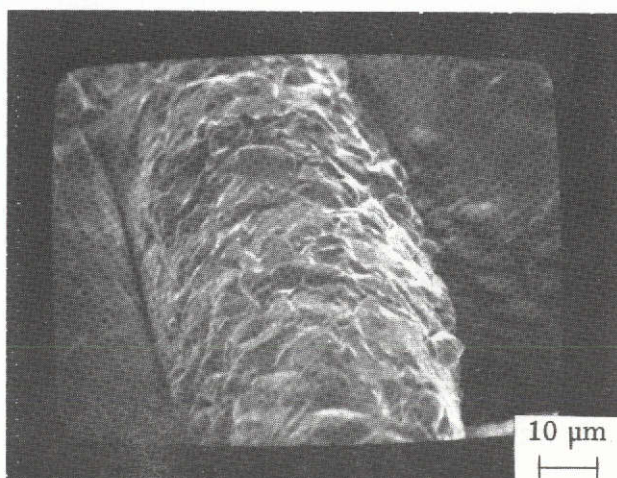
Figure 35. - Thin sputtered tantalum coat-
ing on fine mesh stainless steel wire
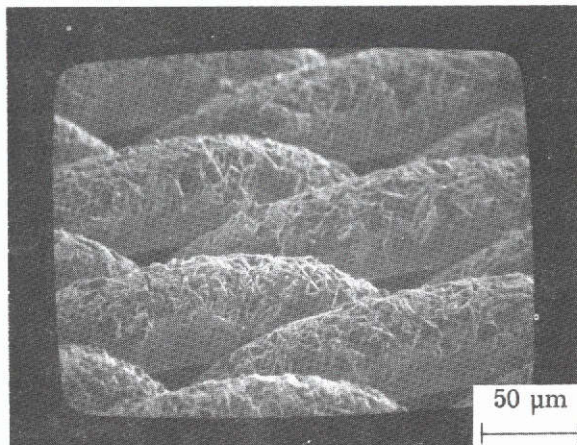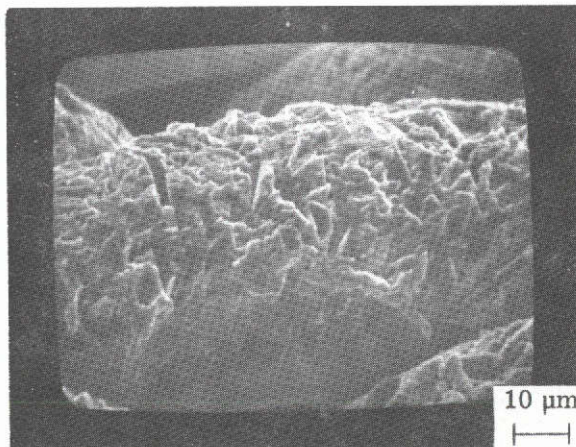cloth grit-blasted at 14 N cm^{-2}. SEM
conditions: 2000 X, 60° tilt.

100 µm
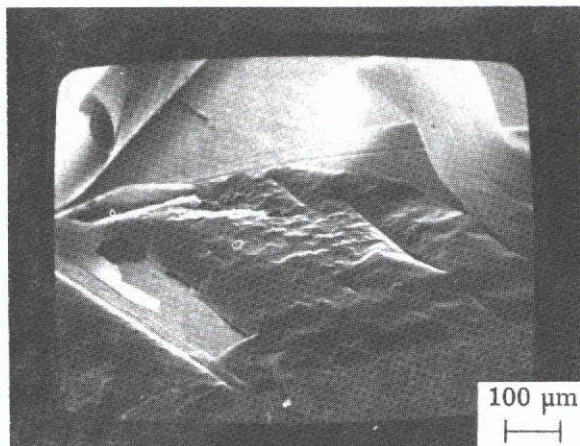
Figure 36. - Sputtered graphite coating on
solid stainless steel specimen grit-
blasted at 14 N cm^{-2}. (Equivalent to
coating from ~10^4 hr small thruster op-
eration.) Note spalling from non-grit-
blasted region to boundary of grit-
blasted region (lower right). SEM con-
ditions: 200 X, 60^0 tilt.

50 µm

(A) SEM conditions: 700 X, 60^0 tilt.

10 µm

(B) SEM conditions: 2000 X, 60^0 tilt.

Figure 37. - Anomalous graphite sputter dep-
osition on fine mesh stainless steel wire
cloth grit-blasted at 14 N cm^{-2}. Note sharp
vertical projections.
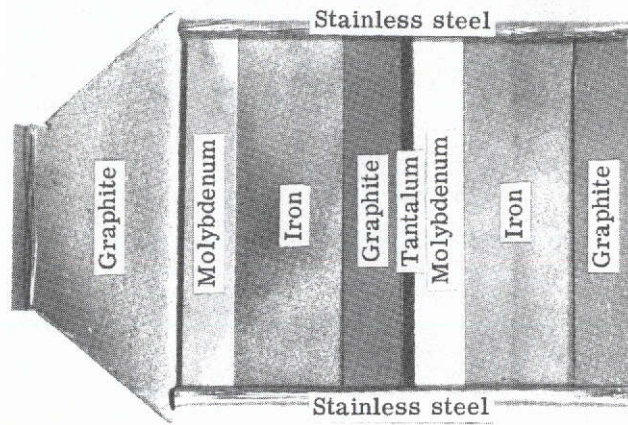
Figure 38. – Composite sputtering target.
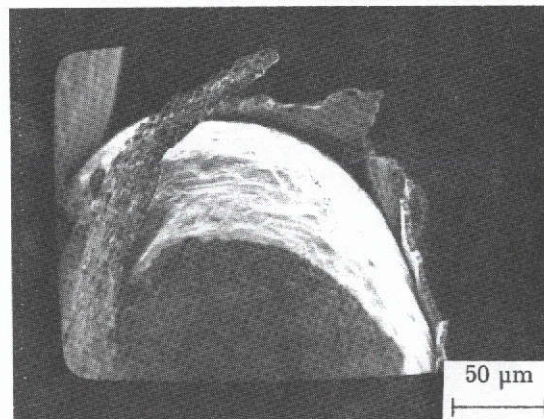
Figure 39. – Sputtered composite coating spalling from non-grit-blasted region of coarse stainless steel wire cloth specimen. (Equivalent to coating from ∼10^4 hr small thruster operation.) SEM conditions: 700 X, 60° tilt.
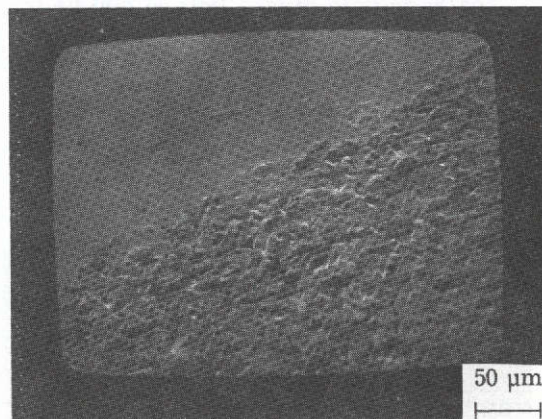

Figure 40. – Sputtered composite coating on solid stainless steel specimen grit-blasted at 28 N cm^{-2}, showing coated area across boundary between grit-blasted region (foreground) and non-grit-blasted region (background). SEM conditions: 500 X, 60° tilt.
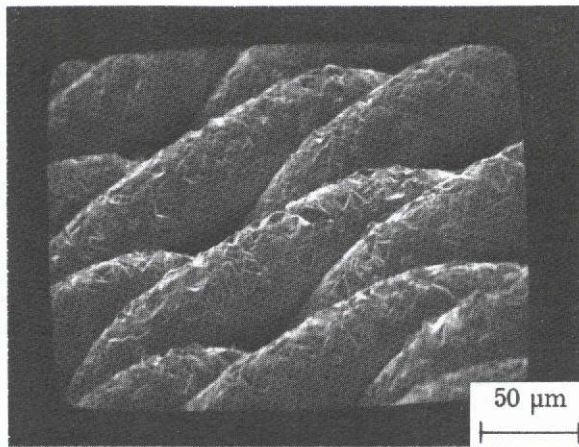
Figure 41. - Anomalous sputtered material deposits on fine mesh stainless steel wire cloth grit-blasted at 14 N cm^{-2} in composite target sputter deposition test. SEM conditions: 700 X, 60° tilt.
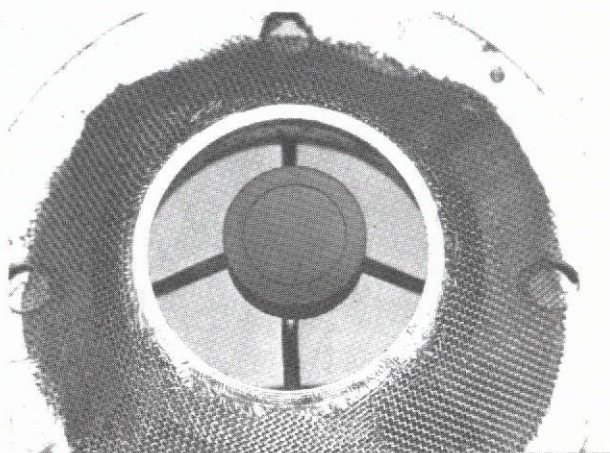

Figure 42. - Thick (2.8 mm) pyrolytic graphite baffle assembly mounted on cathode pole piece, before 400 hr test.
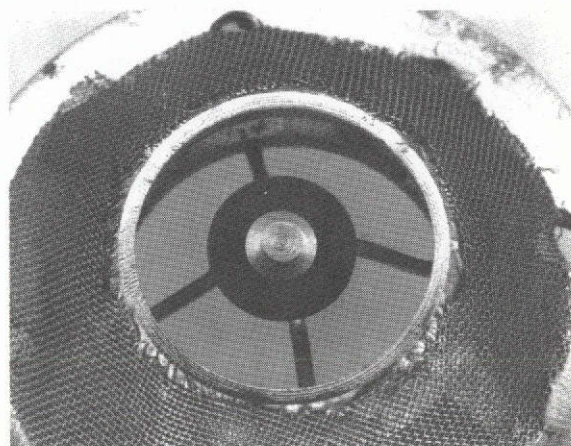

Figure 43. - Thin (0.63 mm) isotropic graphite baffle mounted on cathode pole piece with tantalum mounting screw. Similar to configuration used in cycling life test.